GA 1485 (REV. 4/88)

GENERAL ATOMICS

ISSUE SUMMARY

TITLE: RADIONUCLIDE METHODS VALIDATION WITH FSV DATA

☐ R&D
☒ DV&S
☐ DESIGN

APPROVAL LEVEL 2

DISCIPLINE	SYSTEM	DOC. TYPE	PROJECT	DOCUMENT NO.	ISSUE NO./LTR.
N	11	RGE	6300	DOE-HTGR-88358	0

QUALITY ASSURANCE LEVEL	SAFETY CLASSIFICATION	SEISMIC CATEGORY	ELECTRICAL CLASSIFICATION
N/A	N/A	N/A	N/A

ISSUE	DATE	PREPARED BY	APPROVAL: ENGINEERING	APPROVAL: QA	APPROVAL: FUNDING PROJECT	APPROVAL: APPLICABLE PROJECT	ISSUE DESCRIPTION/ CWBS NO.
0	SEP 29 1989	V. Jovanovic 9-13-89	A. Baxter; R. Turner			G. C. Bramblett	Inital Issue (7652115170) SLPP M/S 5211.5.26

INFO ONLY

DISCLAIMER

CONTINUE ON GA FORM 1485-1

* See list of effective pages

NEXT INDENTURED DOCUMENTS
DOE-HTGR-88312

MASTER

DISTRIBUTION OF THIS DOCUMENT IS UNLIMITED

DISCLAIMER

LIST OF EFFECTIVE PAGES

Page Number	Page Count	Revision
1	1	0
1a	1	0
1b	1	0
2 through 54	53	0
Total Pages	56	

CONTENTS

CONTENTS (CONT'D.)

PAGE

TABLES

FIGURES

CONTENTS (CONT'D.)

PAGE

CONTENTS (CONT'D.)

PAGE

SUMMARY

As part of the radionuclide methods verification program at GA, a fuel performance analysis of the Fort St. Vrain (FSV) core was performed using the reference fuel performance and fission gas release models. The purpose of the analysis was to predict the fuel and graphite temperature distributions, fuel particle failure, and fission gas release as a function of time, and to compare the predicted fission gas release with data taken as part of the FSV radiochemistry surveillance program. The analysis covered the entire operating time of the FSV plant except for the last 18 days prior to the final shutdown because the operating parameters and data for this period were not available when the analysis was performed.

The results of this analysis indicate that very good agreement was obtained between the predicted and measured fission gas release for the key isotopes Kr-85m and Xe-138 during the entire period of analysis. During the first two cycles, excellent agreement has been achieved between the analytical predictions and data, and, for the remaining cycles, the measured fission gas release was overpredicted by less than a factor of two. At the last data point analyzed, the overpredictions of the Kr-85m and Xe-138 release data were by factors of 1.5 and 1.4, respectively. This is considered to be a very good agreement since the required accuracy for fission gas release predictions is a factor of four. This agreement between the analytical predictions and the data serves as a validation of the reference GA fuel failure and fission gas release methods. However, these results indicate that there was still some conservatism in the fission gas release predictions, and that this was likely due to the overprediction of the total coating failure (e.g., exposed kernels) and, to a lesser degree, to the overprediction of fuel temperatures. These results represent an improvement over those of the previous analysis which was based upon the old performance models and which overpredicted the measured Kr-85m release by a larger margin but underpredicted the Xe-138 release.

One interesting observation in the fission gas release data is a significant increase in the release during the last six weeks of the FSV

operation. This increase is most pronounced in the Kr-85m release data and, to a lesser degree, in the Xe-138 data. Prior to this time, the Kr-85m measured data was in a relatively constant range. The increase in the fission gas release is most likely due to an increase in the in-service fuel particle failure which has reached a high enough level to have a noticeable impact on fission gas release, as has been predicted in the analysis; up to this time the predicted in-service fuel particle failure was low and the fission gas release was dominated by the release from as-manufactured heavy-metal contamination of fuel compacts. This increase in the fission gas release during the last six weeks of operation is well predicted by the analysis both with regard to the slope and magnitude of the release.

1. INTRODUCTION

In order to assess the validity of the reference fission gas release methods, a fuel performance analysis of the FSV core during the period from the beginning of cycle 1 (BOC1) to 218.5 effective-full-power days (EFPD) of cycle 4 was conducted in order to predict the fuel and graphite temperature distributions, fuel particle failure, and gaseous fission product release and to compare the predicted fission gas release with data taken during the FSV radiochemistry surveillance program. The time period covered in the analysis includes the entire operating time of the FSV plant except for the last 18 days prior to the final shutdown because the operating parameters and data for this 18-day period were not available when this analysis was performed. The actual operating history was approximated in the analysis by 115 constant power intervals. A comparison was made between the predicted and the available measured fission gas release histories of the key isotopes Kr-85m and Xe-138 in order to assess the validity of these predictions. These calculations are safety related.

The validation of fission metal release and transport methodology was beyond the scope of this effort as no new data was available. Radiochemical examination of the plateout probe during the FSV decommissioning would provide invaluable information for the validation of the GA fission metal release and transport methodology.

2. METHODOLOGY AND ASSUMPTIONS

2.1 Core Power Distribution Analysis

The radial power distributions were calculated for all of the regions and fuel columns with seven calculational points per column, as shown in Figure 1. These results were synthesized with the axial power flux and burnup distributions. The number of time points used in the analysis is given in Tables 1 through 4 for cycles 1 through 4. The results of the core physics calculations were used as input for the thermal and fuel performance analyses.

2.2 Thermal Analysis

Nominal thermal and flow parameters and nominal values of material properties were used in the analysis. The material properties of the fuel element graphite account for thermal expansion and for the effects of fluence and temperature on thermal conductivity and irradiation-induced shrinkage. The model for the thermal conductivity of the fuel compacts, used in the analysis, accounts for the effects of irradiation, temperature and shim content (if any) on the fuel compact thermal conductivity. The thermal conductivity and dimensional change models for graphite and fuel compacts were used to calculate the fuel and graphite temperatures as a function of location and time for the four cycles. The variation of the shim content with the fuel reload segment was taken into account in the analysis; no shim particles were used in the FSV fuel until the fuel segment 8.

The properties of H-327 graphite were used for the entire analysis although half of the fuel segment 9 were made of H-451 graphite. This assumption results in slightly conservative temperatures as the effects of slightly smaller fuel hole gap for the H-327 graphite at elevated temperatures (as a result of less irradiation-induced shrinkage) are more than compensated by the lower thermal conductivity of H-327 compared to H-451.

The core coolant inlet temperature and the total core coolant flow rate were input as a function of time. These values were taken from Tables 1 through 4 (for cycles 1 through 4). The exit coolant temperature deviation, due to mismatch, thermocouple error, etc., was varied with time for each region from BOC1 to 218.5 EFPD's of cycle 4. These values were taken from the data logger tapes. The analysis was performed at the bottom points of all six axial layers of fuel elements.

2.3 Fuel Performance

Typically, the two dominant sources of fission product release from the core are as-manufactured, heavy metal contamination (i.e., heavy metal outside the coated particles) and particles whose coatings fail in service. In addition, the volatile fission metals (Cs and Sr) can, at sufficiently high temperatures and long times, diffuse through the SiC coating and be released from intact TRISO particles.

There are multiple barriers to the release of fission products from an HTGR core: the fuel kernel, the particle coatings, the fuel compact matrix, and the fuel element graphite. The effectiveness of the individual barriers to fission product release may depend upon a number of factors including the chemistry and half-lifes of the various fission products, temperature, and irradiation effects. These barriers are described briefly below.

The first barrier to fission product release is the fuel kernel itself. The kernel of a failed fuel particle retains > 95% of the radiologically important, short-lived fission gases such as Kr-85m and I-131; however, the effectiveness of the fuel kernel for retaining gases can be reduced if the exposed kernel is hydrolyzed by reaction with trace amounts of water vapor which may be present in the helium coolant. The retentivity of fuel kernels for long-lived, volatile fission metals such as Cs and Sr is strongly dependent upon the temperature and the burnup.

The primary barrier to fission product release from the core is the silicon carbide and/or pyrocarbon coatings of each fuel particle. Both the SiC and outer pyrocarbon (OPyC) coatings provide a barrier to the release of

fission gases. The SiC coating acts as the primary barrier to the release of metallic fission products because of the low diffusion coefficients of these metals in SiC; the OPyC coating is partially retentive of Cs at lower temperatures but provides little holdup of Sr.

The fuel compact matrix is rather porous and provides little holdup of the fission gases which are released from the fuel particles. However, the matrix is a composite material which has a high content of amorphous carbon, and this constituent of the matrix is highly sorptive of metallic fission products, especially Sr. While the matrix is highly sorptive of metals, it provides little diffusional resistance to the release of fission metals because of its high interconnected porosity.

The fuel element graphite, which is denser and has a more ordered structure than the fuel compact matrix, is somewhat less sorptive of the fission metals than the matrix, but it is much more effective as a diffusion barrier than the latter. The effectiveness of the graphite as a release barrier decreases as the temperature increases. Under typical FSV core conditions, the fuel element graphite attenuates the release of Cs and from the core by more than an order of magnitude, and the Sr is essentially quantitatively retained.

The above discussion applies to the transport of fission products that are produced in the kernels of intact particles. Obviously, fission products resulting from fissions in heavy-metal contamination outside of the particles are not attenuated by the kernels or coatings, nor are the fission products produced in the kernels of failed particles appreciably attenuated by the failed coatings.

The performance of coated fuel particles is calculated by models defining several potential failure mechanisms. The HTGR fuel performance models calculate fission product release to the reactor coolant during normal operation from the following seven sources:

1. Coating damage during fuel manufacture, resulting in heavy metal contamination on coating surfaces and in the fuel

compact matrix.

2. Pressure vessel failure in particles with defective or missing coating layers.

3. Pressure vessel failure in standard particles, i.e., particles without manufacturing defects.

4. Irradiation-induced failure of outer pyrocarbon coating as function of fluence in both standard and defective particles.

5. Failure of the SiC coating caused by fission product/SiC interaction.

6. Failure of the SiC coating by thermal decomposition.

7. Failure of the SiC coating due to kernel migration in the presence of a thermal gradient.

The models for predicting fission gas release from heavy-metal contamination and failed particles give the release rate-to-birth rate ratios (R/B) from failed particles and contamination as a function of chemical element, isotope half-life, temperature, and burnup. In addition, the effect of fuel hydrolysis, or reaction of exposed fuel kernels with water, on gas release is included.

The methodology described here was used to predict the fuel performance and fission product release for the FSV core. The application of this performance methodology is described in the following sections.

2.3.1 Fuel Particle Failure

Using the calculated fuel temperature histories (Section 2.2), burnup and fast fluence histories, and fuel performance models, the fuel particle failures were calculated as a function of time. The particle failures from

the aforementioned mechanisms were calculated at the 50% confidence level.

Of particular importance to the subject analysis is that fuel particles, especially the fertile particles, in segments 1-7 had OPyC coatings with high microporosities. Based upon the results of accelerated fuel irradiation capsules and fuel test elements in Peach Bottom 1, very high failure rates (>30%) for these OPyC coatings at a modest fast fluence of 2×10^{25} n/m^2 were predicted previously. This original failure model was too conservative, and its use resulted in an overprediction of the fission gas release data. Consequently, the data base was reexamined for the OPyC failure for the FSV fuel compacts. Since the conservatism in the model was due to the inclusion of nonrepresentative irradiation data, the OPyC performance model was revised by including only the data for the fuel compacts made with FSV production materials, and the revised model was used in this analysis. The variation of the fuel quality with service limit, fuel segment and axial location was taken into account in the analysis.

2.3.2 Gaseous Fission Product Release

The detailed results were averaged radially and axially in order to obtain core-average results. The gaseous fission product releases were calculated for the two key isotopes Kr-85m and Xe-138. These isotopes were also selected for analysis because their predicted releases can be directly compared with measurements taken as part of the FSV radiochemistry surveillance program. The fission gas release measurements were obtained from Refs. 1 and 2.

In calculating the fission gas release, it was assumed that the performance models for the UC_2 fuel particles apply to the $(Th/U)C_2$ and ThC_2 fuel particles. The fission gas release model was revised in that the temperature enhancement term was eliminated because it has been shown to be excessively conservative for steady-state reactor operation. The diffusion parameter for the release of xenon from heavy-metal contamination was also revised because the use of the original value resulted in an underprediction of the xenon release for the FSV core at the beginning of cycle 1 when the entire release is from the heavy-metal contamination; the revised value is

based upon the available experimental data. For the calculation of the fission gas release due to as-manufactured heavy-metal contamination of the fuel compacts, the thorium and uranium contamination fractions were taken from the QC records for the initial core and reload segments. Nominal values for the material properties were used in the calculations.

The releases for other fission gases can be obtained by assuming that the release rate-to-birth rate ratio (R/B) varies as the square root of isotope half-life. Moreover, it is assumed that bromine and selenium isotopes have the same release characteristics as krypton isotopes and that iodine and tellurium isotopes have the same release characteristics as xenon.

3. RESULTS AND DISCUSSION

3.1 Fuel and Graphite Temperatures

Although the analysis was performed for the entire active core, the fuel and graphite temperature predictions are presented only for the fuel segments 1 and 7; the latter was chosen because the maximum fuel and graphite temperatures were predicted to occur in a fuel element belonging to this segment, and the former represents a "typical" initial core fuel segment regarding the fuel and graphite temperatures. The regions that belong to the fuel segment 1 (and the refueling segment 7) include the regions 5, 10, 17, 21, 28, and 35 (see Fig. 1). The volume distributions of the predicted fuel and graphite temperatures are presented in Figures 2 through 5 for the fuel segments 1 and 7; the figures show the distributions of the peak and time-averaged temperatures.

The largest temperatures were predicted to occur at a few locations on the outer boundary of the active core at the corners of the fuel elements surrounded on both sides by reflector elements and in every case in reloaded fuel elements. At these peripheral locations very large point power factors and power tilts were calculated in the core physics analysis for both partially buffered and fully buffered fuel elements. In case of partially buffered fuel elements, the core physics analysis can overestimate such point power factors and tilts by some 15%. For the fully buffered fuel elements, the core physics analysis with the seven-group cross-sections, as used for cycles 2, 3 and 4, calculates such point power factors that are some 20% higher than with the four-group cross-sections; the use of the latter is considered to give more realistic representation at such points at the reflector boundary interface. Also, the thermal analysis overestimates graphite temperatures at such points since it does not account for convective losses to the gap flow and for the radiative losses to the adjacent reflector elements.

A previous detailed thermal analysis of such fuel elements indicated that, due to physics modeling difficulties, the predicted intercolumn power tilts in partially buffered fuel elements can be excessively conservative,

resulting in significant overpredictions of fuel and graphite temperatures, as was the case in this analysis. Even though these temperatures are excessive, they were included in the analysis since they are the result of the current core physics methodology and since their use results in clearly conservative predictions of temperature-induced fuel failure and fission product release.

For the entire core, the peak and time-averaged maximum fuel temperatures of 1442°C (2628°F) and 1054°C (1930°F) were predicted, as shown in Figures 2 and 3. These maximum temperatures were predicted to occur in the fuel segment 7, region 28, column 5, local point 5, which is a point in a partially buffered fuel element (see Fig. 1 for the region, column and local point designation). The peak graphite temperature was predicted to be 1395°C (2543°F) and 1025°C (1877°F) on time-average basis, as shown in Figures 4 and 5. These maximum temperatures were predicted to occur at the bottom of the active core. Somewhat lower fuel and graphite temperatures were predicted for segments 8 and 9, again at the outer radial boundary and the bottom of the active core and several days after the reload. It should be emphasized that only very small fractions of fuel and graphite volumes in the reload segments were predicted to reach such high temperatures, as can be seen in the figures.

3.2 Burnup and Fluence Distributions

Fuel volume distributions of fissile and fertile particle burnup for segments 1 through 6 are shown in Figures 6 through 17. At the last time point (corresponding to 218.5 EFPD's of cycle 4), the maximum fissile and fertile burnups were less than 0.16 and 0.035 FIMA, respectively. The maximum burnups occur in fuel segments 4, 5 and 6 because these segments are not reloaded during the first four cycles, and thus their fuel has a longer residence time than other fuel segments. These values are lower than the design values of the fissile and fertile burnup of 0.2 and 0.07 FIMA, respectively.

Fuel volume distributions of fast neutron fluence for segments 1 and 6 are shown in Figures 18 through 23. Again, the maximum fluence is reached

in fuel segments 4, 5 and 6. The maximum value was less than 4.5×10^{25} n/m^2, which is lower than the design value of 8×10^{25}.

3.3 Fuel Particle Failure Predictions

Time histories of the core-averaged fuel particle failures are shown in Fig. 24 and 25 for the fissile and fertile fuels, respectively. These failures are based on the reference fuel particle failure models and revisions thereof, as discussed in Section 2.3. These failure models account for partially failed fuel particles, i.e. particles with failed SiC but intact OPyC coatings, which are assumed to retain fission gases but to release fission metals. Accordingly, two sets of failure fractions are shown in Fig. 24 and 25. For the fissile particles, the maximum predicted core-averaged fuel particle failures were 0.041% and 0.350% for the particles with exposed kernels (resulting in fission gas release) and failed SiC coatings (resulting in fission metal release), respectively. For the fertile particles, the maximum predicted fuel particle failures were 0.090% and 1.25% for the particles with exposed kernels and failed SiC coatings, respectively.

3.4 Gaseous Fission Product Release Predictions

The predicted release rate-to-birth rate ratios (R/Bs) or fractional releases for the two reference fission gases Kr-85m and Xe-138 are shown in Fig. 26 and 27 as a function of time. The predicted fission gas releases at the last time point analyzed (218.5 EFPD's of cycle 4) are shown in Table 1 along with the contributions from failed fissile and fertile particles and the as-manufactured heavy-metal contamination to the total release. The predicted R/Bs for Kr-85m and Xe-138 were 2.0×10^{-5} and 2.2×10^{-6}, respectively.

4. COMPARISON OF PREDICTED AND MEASURED FISSION PRODUCT RELEASE

A comparison was made between the predicted and the available measured fission gas release histories of Kr-85m and Xe-138, as shown in Fig. 28 and 29. This comparison indicates that very good agreement was obtained between the predicted and measured fission gas release for the key isotopes Kr-85m and Xe-138 during the entire period of analysis. During the first two cycles, excellent agreement has been achieved between the analytical predictions and data, and, for the remaining cycles, the data were overpredicted by less than a factor of two. At the last data point analyzed, the overpredictions of the Kr-85m and Xe-138 release data were by factors of 1.5 and 1.4, respectively. However, these results indicate that there was still some conservatism in the fission gas release predictions, and that this was likely due to the overprediction of the total coating failure (e.g., exposed kernels) and, to a lesser degree, to the overprediction of fuel temperatures. These results represent an improvement over those of the previous analysis which was based upon the old fuel performance models and which overpredicted the measured Kr-85m release by a larger margin but underpredicted the Xe-138 release. Also included in Fig. 28 and 29 are the FSV FSAR (Ref. 3) "Expected" values which indicate that both the Kr-85m and Xe-138 releases were well below the "Expected" values.

One interesting observation in the fission gas release data is a significant increase in the release during the last six weeks of the FSV operation. This increase is most pronounced in the Kr-85m release data and, to a lesser degree, in the Xe-138 data. Prior to this time, the Kr-85m measured data were in a relatively constant range. The increase in the fission gas release is most likely due to an increase in the in-service fuel particle failure which has reached a high enough level to have a noticeable impact on fission gas release, as has been predicted in the analysis; up to this time the predicted in-service fuel particle failure was low and the fission gas release was dominated by the release from as-manufactured heavy-metal contamination of fuel compacts. This increase in the fission gas release during the last six weeks of operation is well predicted by the analysis both with regard to the slope and magnitude of the release.

5. CONCLUSIONS

The results of this analysis, based on the reference fuel failure and fission gas release models, indicate that very good agreement was obtained between the predicted and measured fission gas release for the key isotopes Kr-85m and Xe-138 during the entire period of analysis. During the first two cycles, excellent agreement has been achieved between the analytical predictions and data, and, for the remaining cycles, the data were overpredicted by less than a factor of two. At the last data point analyzed, the overpredictions of the Kr-85m and Xe-138 release data were by factors of 1.5 and 1.4, respectively. This is considered to be a very good agreement since the required accuracy for fission gas release predictions is a factor of four. This agreement between the analytical predictions and the data serves as a validation of the fuel failure and fission gas release methods.

6. REFERENCES

1. Montgomery, F. C. and R. D. Burnette, "FSV Cycle 4 Coolant Chemistry and Tritium Sorption on Moderator Graphite," DOE Report HTGR-86-079, September 1986.

2. Burnette, R. D., "Test Status Report on Fort St. Vrain HTGR Coolant and Radiochemistry: July 1983 Through June 1984," General Atomics Document 907650/1, September 28, 1984.

3. Public Service Company of Colorado, "Fort St. Vrain Nuclear Generating Station FSAR," Section 3.7.

Table 1

THERMAL POWER, FLOW AND CORE INLET TEMPERATURE HISTORIES FOR FSV CYCLE 1

Time Point	EFPD	Thermal Power(%)	Power/Flow	Core Inlet Temperature (°F)
1	0	5.0	0.568	550.0
2	3.0	23.5	0.553	593.2
3	4.6	27.7	0.722	631.2
4	12.8	29.7	0.803	640.3
5	19.0	49.3	0.672	611.1
6	20.0	28.9	0.698	616.6
7	26.0	27.9	0.622	584.8
8	26.7	28.7	0.736	614.7
9	28.6	28.6	0.689	613.9
10	30.5	28.4	0.751	619.4
11	33.8	38.7	0.791	626.4
12	38.8	36.5	0.804	622.5
13	51.7	29.6	0.781	636.9
14	53.0	54.6	0.870	659.1
15	57.4	25.4	0.868	636.2
16	62.8	34.0	0.731	619.3
17	68.9	51.1	0.842	651.4
18	72.9	65.3	0.915	659.1
19	77.0	30.5	0.782	633.3
20	79.7	65.3	0.916	664.4
21	87.2	61.5	0.797	637.9
22	89.7	61.5	0.837	653.0
23	92.5	63.5	0.904	658.8
24	102.3	22.8	0.626	653.2
25	103.1	38.0	0.778	633.2
26	105.2	62.9	0.870	669.4
27	113.7	51.2	0.838	649.5
28	115.9	28.6	0.615	627.3
29	120.0	49.3	0.862	643.9
30	123.5	2.1	0.862	643.9
31	123.5	36.1	0.742	609.6
32	128.3	12.0	0.655	568.9
33	129.5	53.7	0.909	644.9
34	136.6	53.3	1.002	654.3
35	144.9	64.8	0.929	656.3
36	173.4	35.2	0.929	656.3

Full power = 841.7 MW(t)
Full flow = 3.49×10^6 lb/hr

Table 2

THERMAL POWER, FLOW AND CORE INLET TEMPERATURE HISTORIES FOR FSV CYCLE 2

Time Point	EFPD	Thermal Power(%)	Power/Flow	Core Inlet Temperature (°F)
1	0	0		
2	0	47.4	0.739	637.8
3	4.66	65.1	0.896	668.1
4	8.11	65.2	0.874	665.0
5	13.13	40.4	0.706	637.8
6	15.88	20.2	0.483	530.0
7	16.90	32.1	0.793	637.7
8	18.35	53.4	0.766	654.4
9	23.72	66.0	0.889	673.1
10	36.77	33.8	0.683	631.2
11	43.41	55.8	0.876	638.0
12	60.30	69.7	0.884	667.6
13	70.06	52.5	0.830	635.9
14	81.15	43.1	0.746	621.5
15	84.04	55.7	0.834	612.2
16	90.16	44.6	0.782	647.6
17	95.28	59.0	0.912	671.9
18	96.69	46.7	0.717	677.5
19	101.14	63.9	0.909	674.9
20	108.87	68.9	0.961	672.5
21	123.82	43.7	0.797	643.6
22	126.79	69.2	0.888	677.6
23	132.19	38.0	0.777	642.7
24	138.44	55.8	0.754	678.1
25	140.95	68.3	0.892	678.5
26	145.83	69.7	0.848	690.2
27	157.33	39.5	0.738	635.4
28	163.51	69.3	0.871	686.1
29	168.35	47.2	0.770	649.9
30	170.48	80.3	0.880	695.1
31	174.95	70.0	0.859	680.9
32	188.71	70.0	0.859	680.9

Full power = 841.7 MW(t)
Full flow = 3.49×10^6 lb/hr

Table 3

THERMAL POWER, FLOW AND CORE INLET TEMPERATURE HISTORIES FOR FSV CYCLE 3

Time Point	EFPD	Thermal Power(%)	Power/Flow	Core Inlet Temperature (°F)
1	0	70.2	0.882	680.2
2	18.99	69.4	0.907	671.0
3	39.70	68.3	0.916	653.7
4	44.48	34.6	0.718	599.4
5	50.71	5.9	0.274	360.5
6	50.92	68.3	0.892	677.3
7	52.97	100.0	0.906	737.9
8	55.47	69.9	0.892	677.3
9	71.29	70.2	0.892	677.3
10	85.40	69.6	0.920	667.2
11	105.31	69.6	0.868	677.9
12	123.41	69.6	0.856	680.8
13	146.68	70.1	0.878	677.9
14	153.26	70.1	0.897	688.9
15	165.18	26.1	0.528	617.3
16	167.45	26.1	0.528	617.3
17	170.44	42.4	0.828	625.9
18	187.47	61.8	0.992	704.5
19	207.68	65.9	0.868	684.2
20	228.29	69.4	0.884	684.0
21	247.49	32.8	0.558	653.7
22	251.02	70.7	0.874	690.9
23	268.18	70.0	0.860	691.2
24	282.70	67.5	0.886	685.2
25	293.75	30.3	0.662	639.6
26	294.62	30.3	0.662	639.6

Full power = 841.7 MW(t)
Full flow = 3.49×10^6 lb/hr

Table 4

THERMAL POWER, FLOW AND CORE INLET TEMPERATURE HISTORIES
FOR FSV CYCLE 4 TO 218.5 EFPD

Time Point	EFPD	Thermal Power(%)	Power/Flow	Core Inlet Temperature (°F)
1	0.0	28.5	0.628	648.0
2	4.9	9.0	0.331	376.6
3	8.9	26.6	0.532	639.1
4	13.0	33.9	0.702	646.4
5	15.6	34.5	0.725	644.0
6	17.4	30.0	0.674	629.9
7	20.7	30.1	0.672	620.4
8	24.9	29.1	0.705	627.1
9	41.8	57.0	0.830	661.0
10	56.8	29.7	0.731	628.5
11	59.1	71.3	0.935	675.0
12	82.9	29.7	0.745	620.4
13	86.9	77.2	0.978	684.0
14	116.5	79.6	0.943	688.7
15	154.7	28.5	0.679	604.0
16	160.4	50.5	0.770	656.2
17	165.1	68.3	0.860	677.5
18	180.1	79.1	0.916	688.4
19	184.9	79.0	0.893	697.4
20	194.4	79.0	0.890	700.8
21	218.5	79.0	0.885	700.7

Full power = 841.7 MW(t)
Full flow = 3.49×10^6 lb/hr

Table 5

FSV PREDICTED CORE-AVERAGED FISSION GAS RELEASES

AT 218.5 EFPD'S OF CYCLE 4

Kr-85m

Total Predicted R/B, Hydrolyzed Fuel	2.0×10^{-5}
% R/B Due to failed fertile particles	50.7
% R/B Due to failed fissile particles	23.4
% R/B Due to as-manufactured heavy-metal contamination	25.9

Xe-138

Total Predicted R/B, Hydrolyzed Fuel	2.2×10^{-6}
% R/B Due to failed fertile particles	19.0
% R/B Due to failed fissile particles	21.0
% R/B Due to as-manufactured heavy-metal contamination	60.0

Figure 1

FSV CORE

Region Identification Numbers

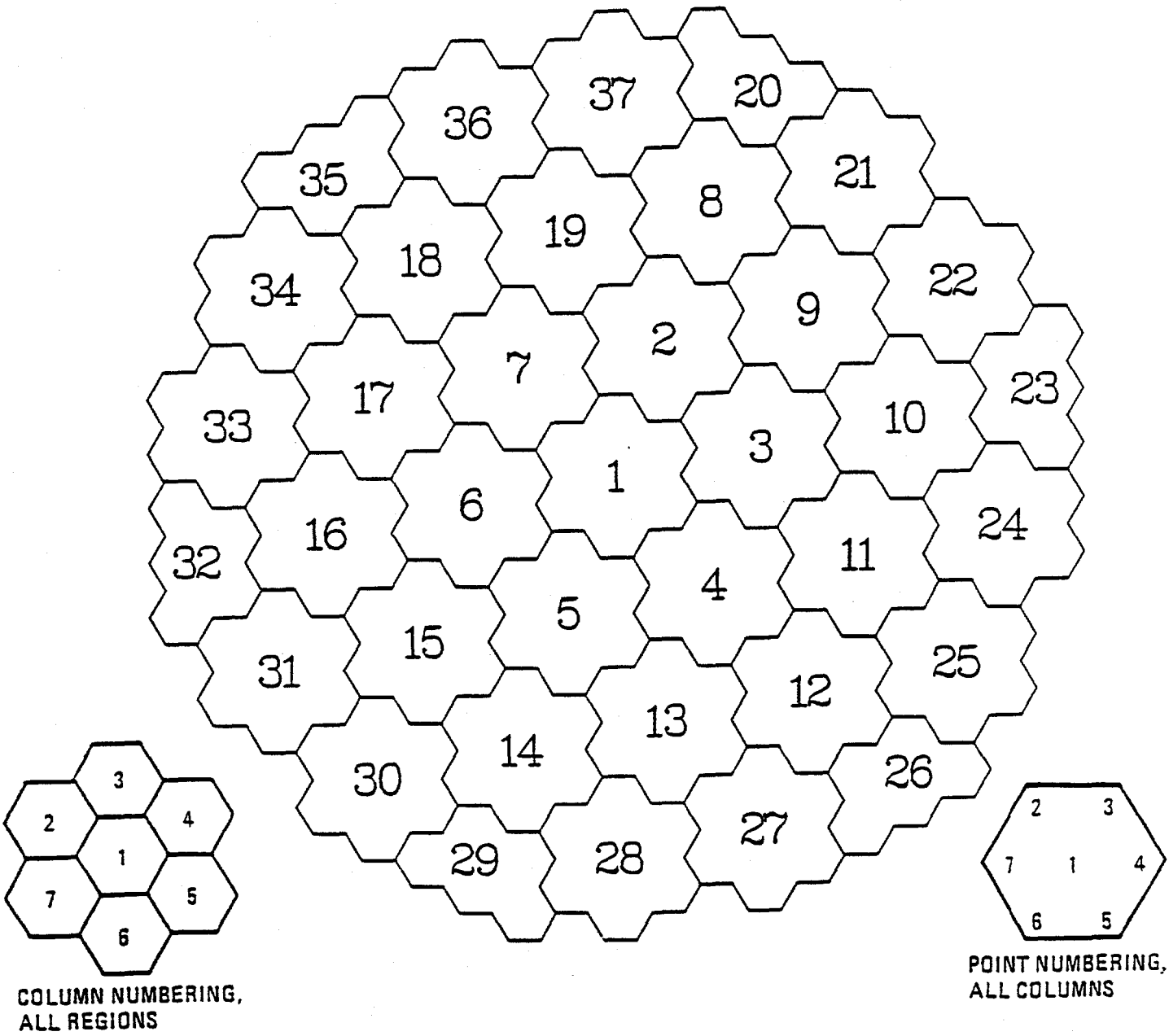

COLUMN NUMBERING, ALL REGIONS

POINT NUMBERING, ALL COLUMNS

Figure 2
PEAK FUEL TEMPERATURE VOLUME DISTRIBUTIONS
FOR SEGMENTS 1 AND 7

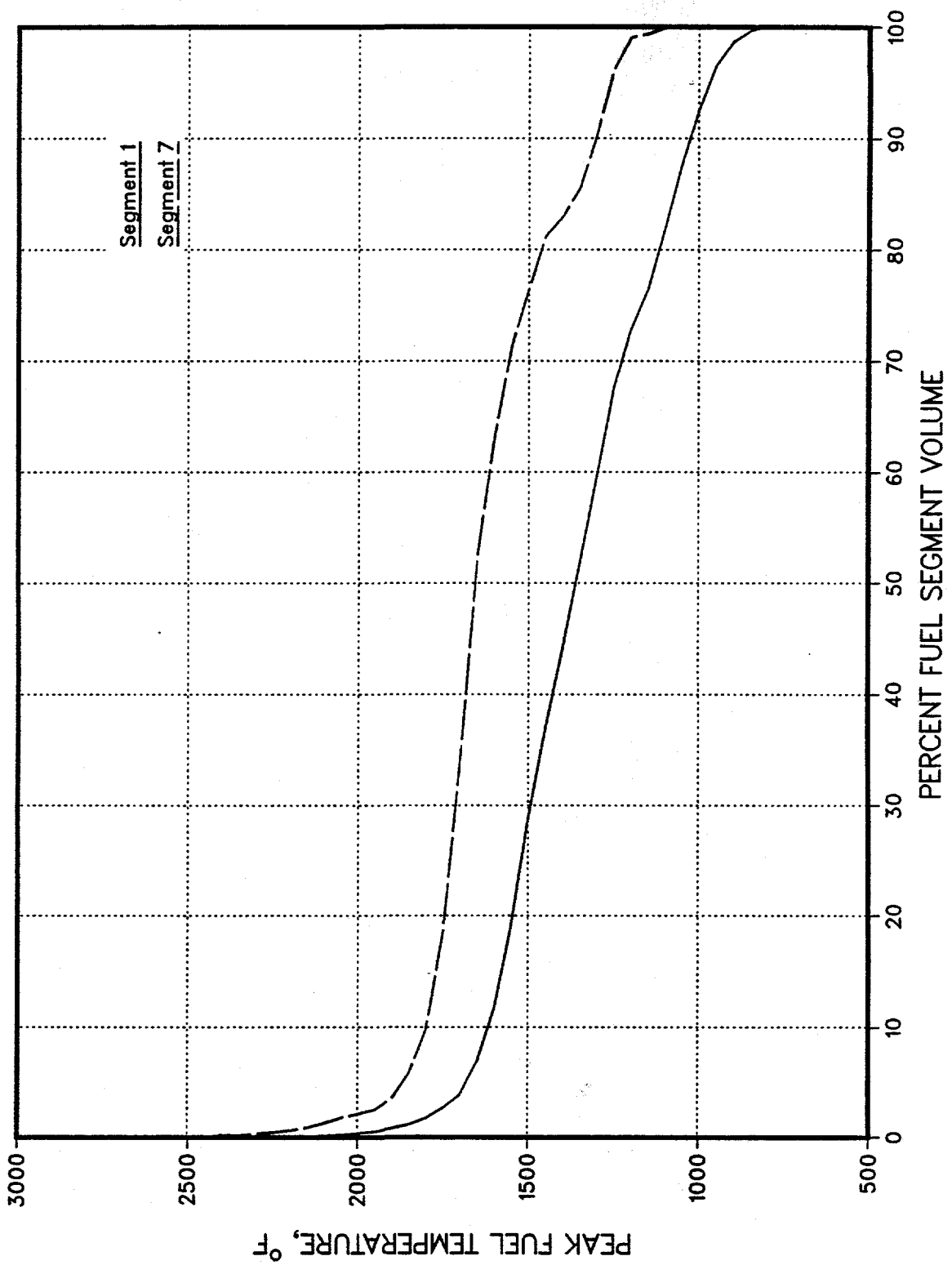

Figure 3

TIME-AVERAGED FUEL TEMPERATURE VOLUME DISTRIBUTIONS FOR SEGMENTS 1 AND 7

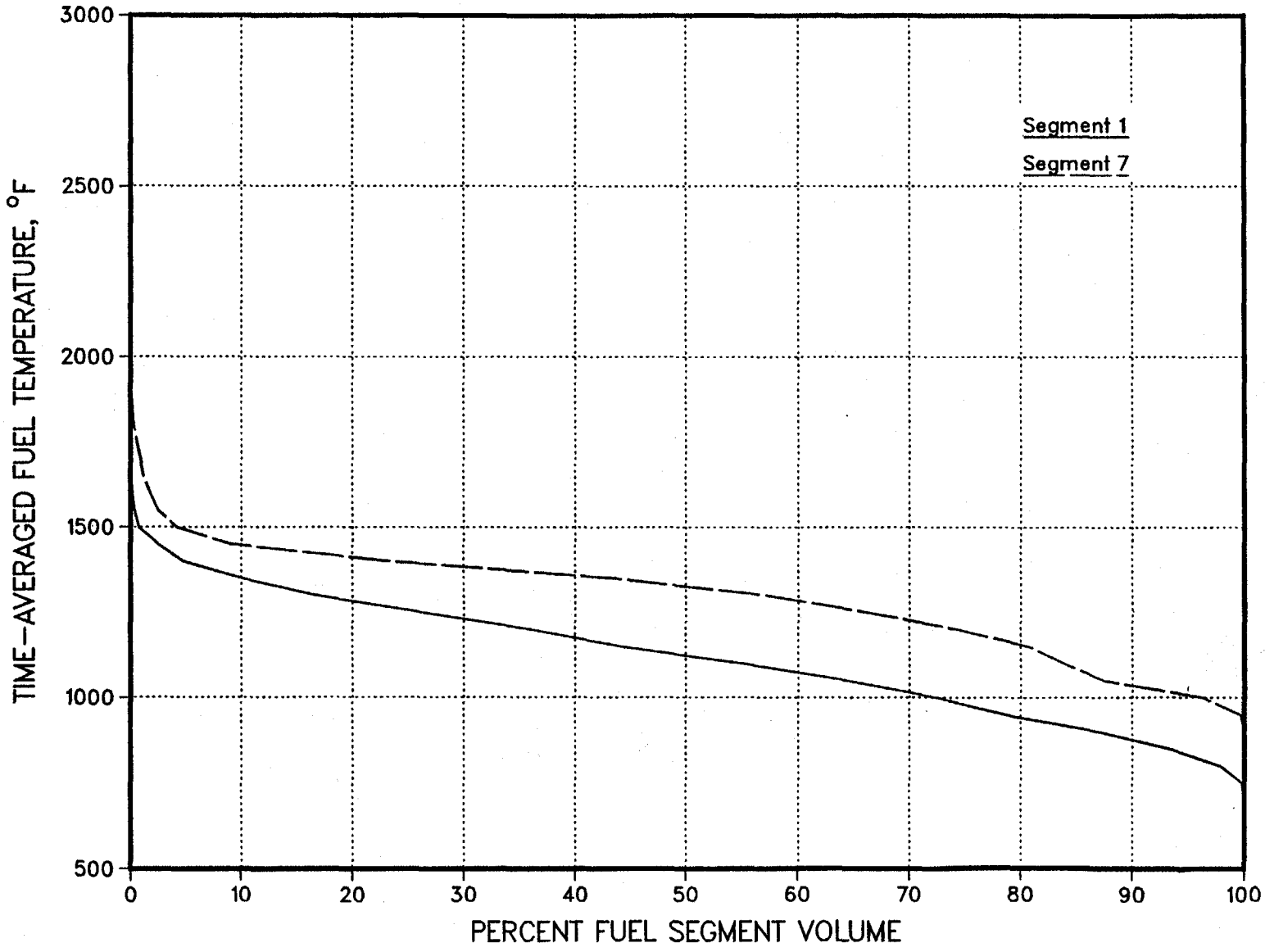

Figure 4
PEAK GRAPHITE TEMPERATURE VOLUME DISTRIBUTIONS
FOR SEGMENTS 1 AND 7

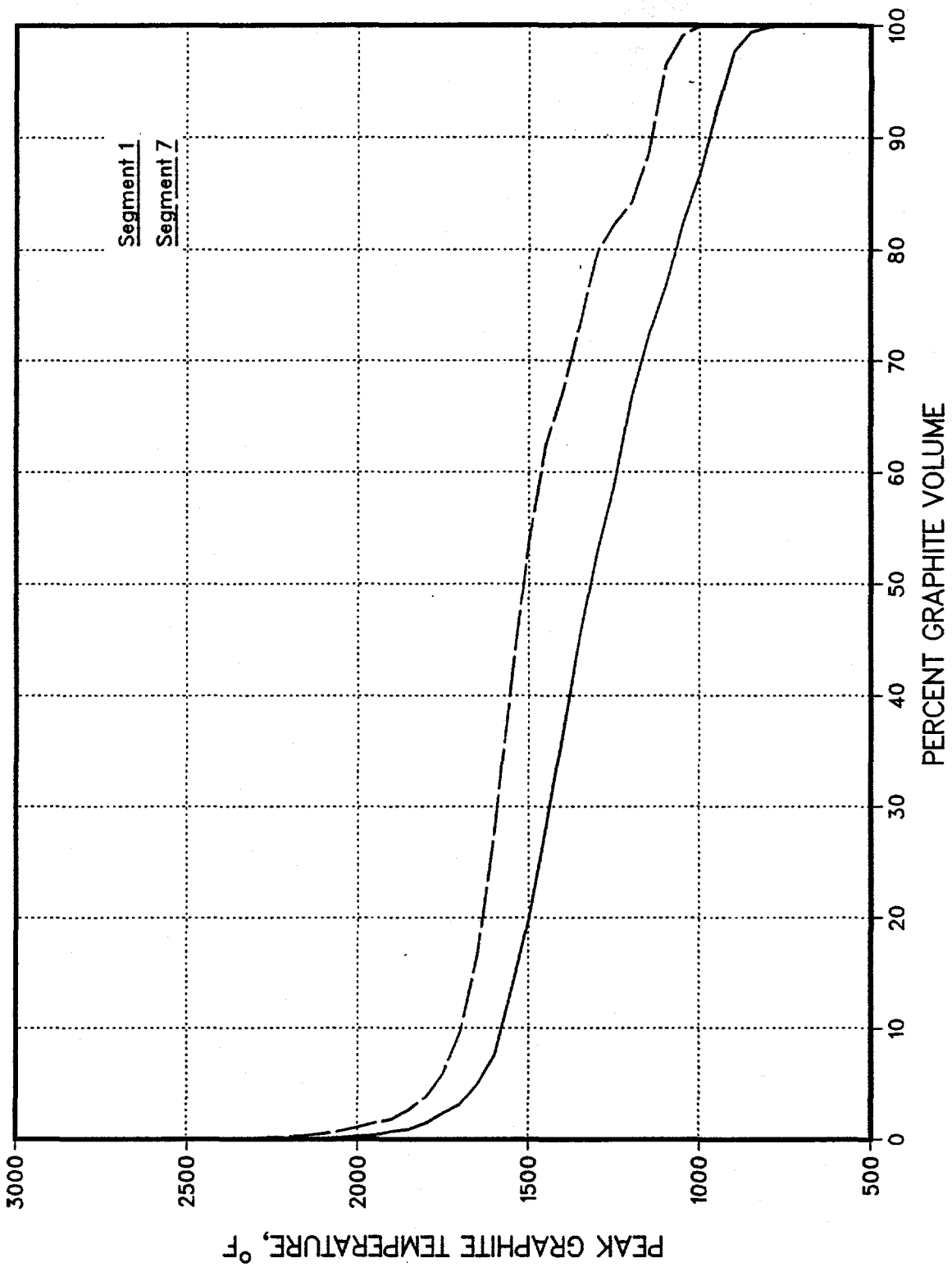

Figure 5
TIME-AVERAGED GRAPHITE TEMPERATURE VOLUME DISTRIBUTIONS
FOR SEGMENTS 1 AND 7

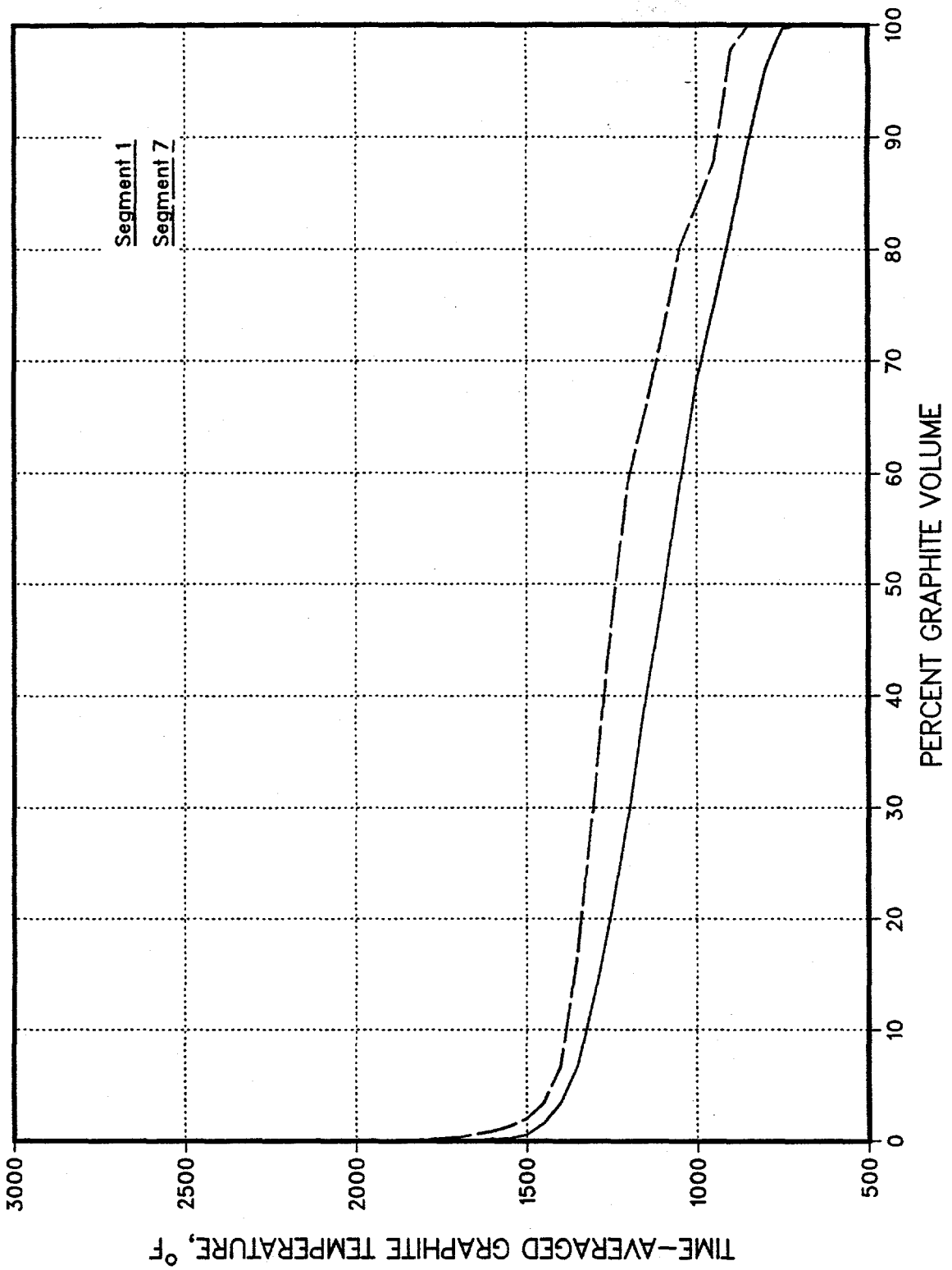

Figure 6
FISSILE BURNUP VOLUME DISTRIBUTIONS FOR SEGMENTS 1 AND 7

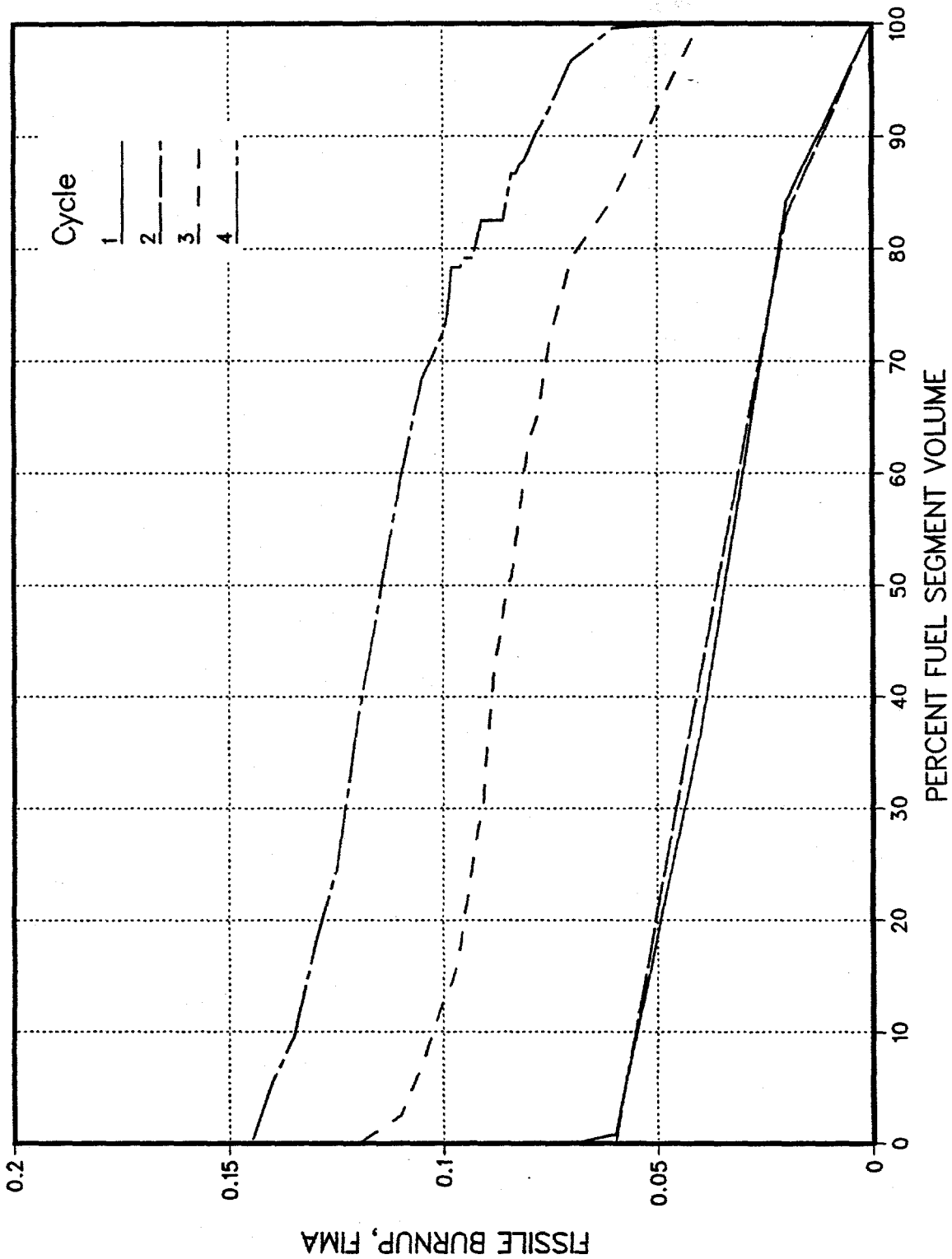

Figure 7
FERTILE BURNUP VOLUME DISTRIBUTIONS FOR SEGMENTS 1 AND 7

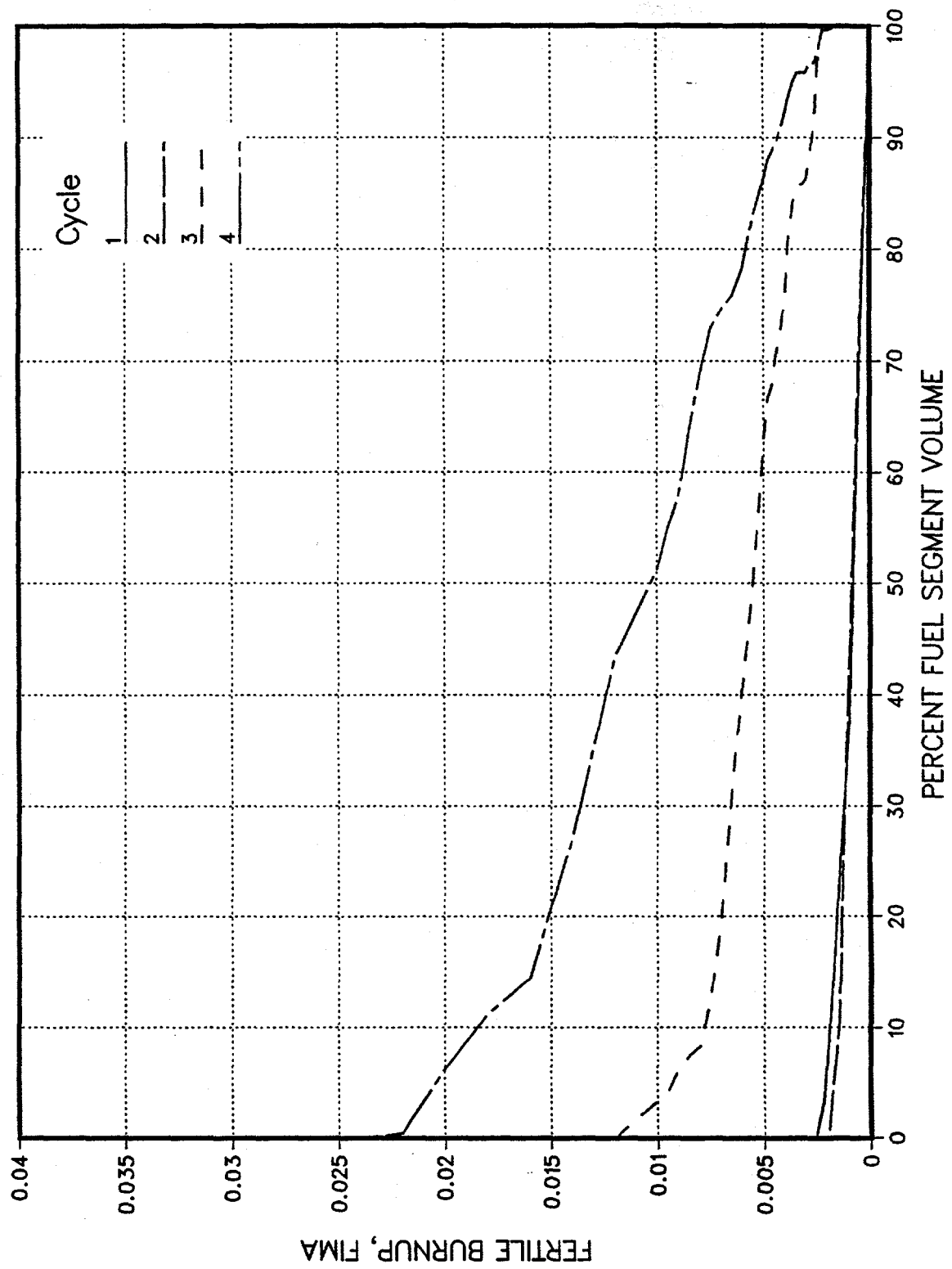

Figure 8
FISSILE BURNUP VOLUME DISTRIBUTIONS FOR SEGMENTS 2 AND 8

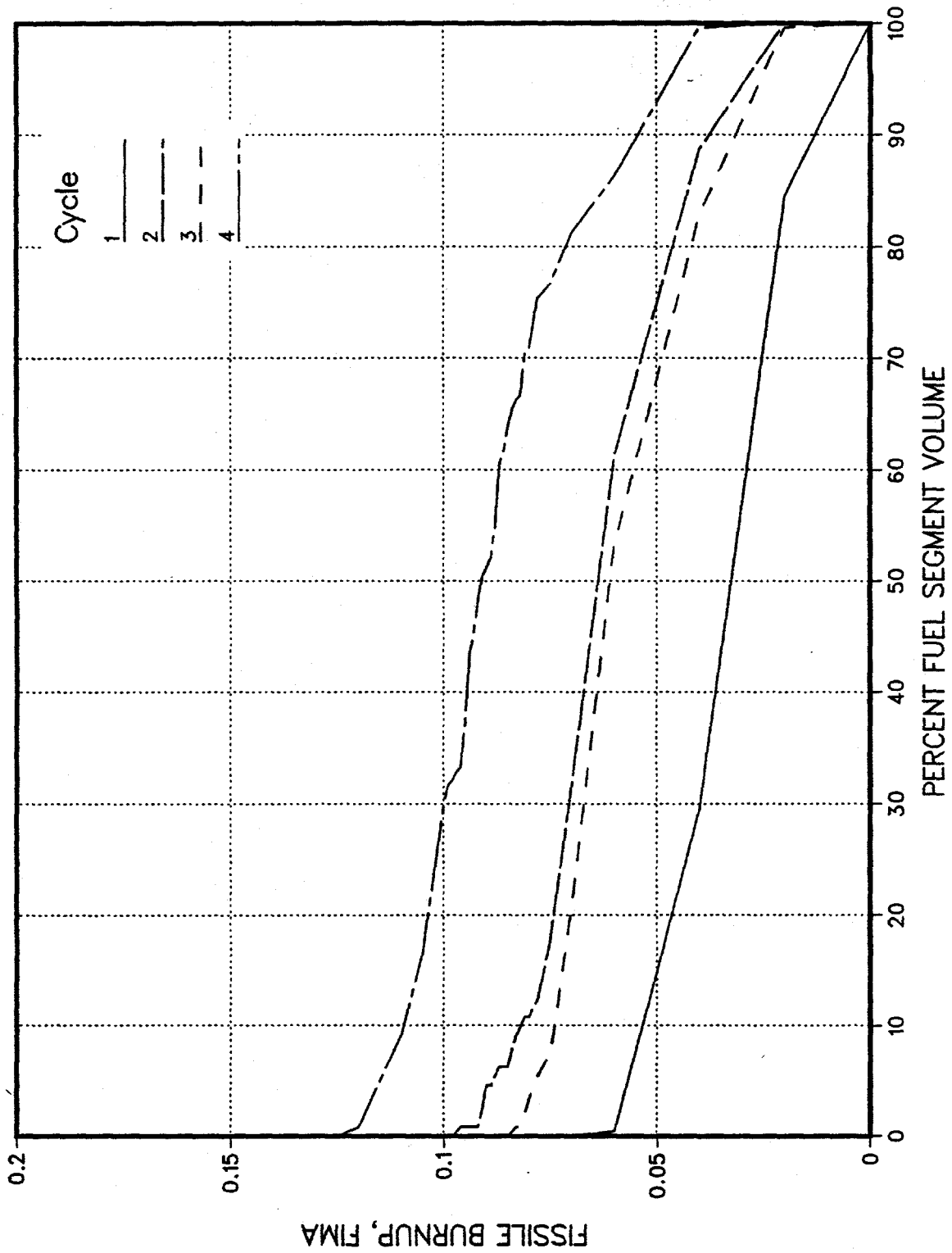

Figure 9
FERTILE BURNUP VOLUME DISTRIBUTIONS FOR SEGMENTS 2 AND 8

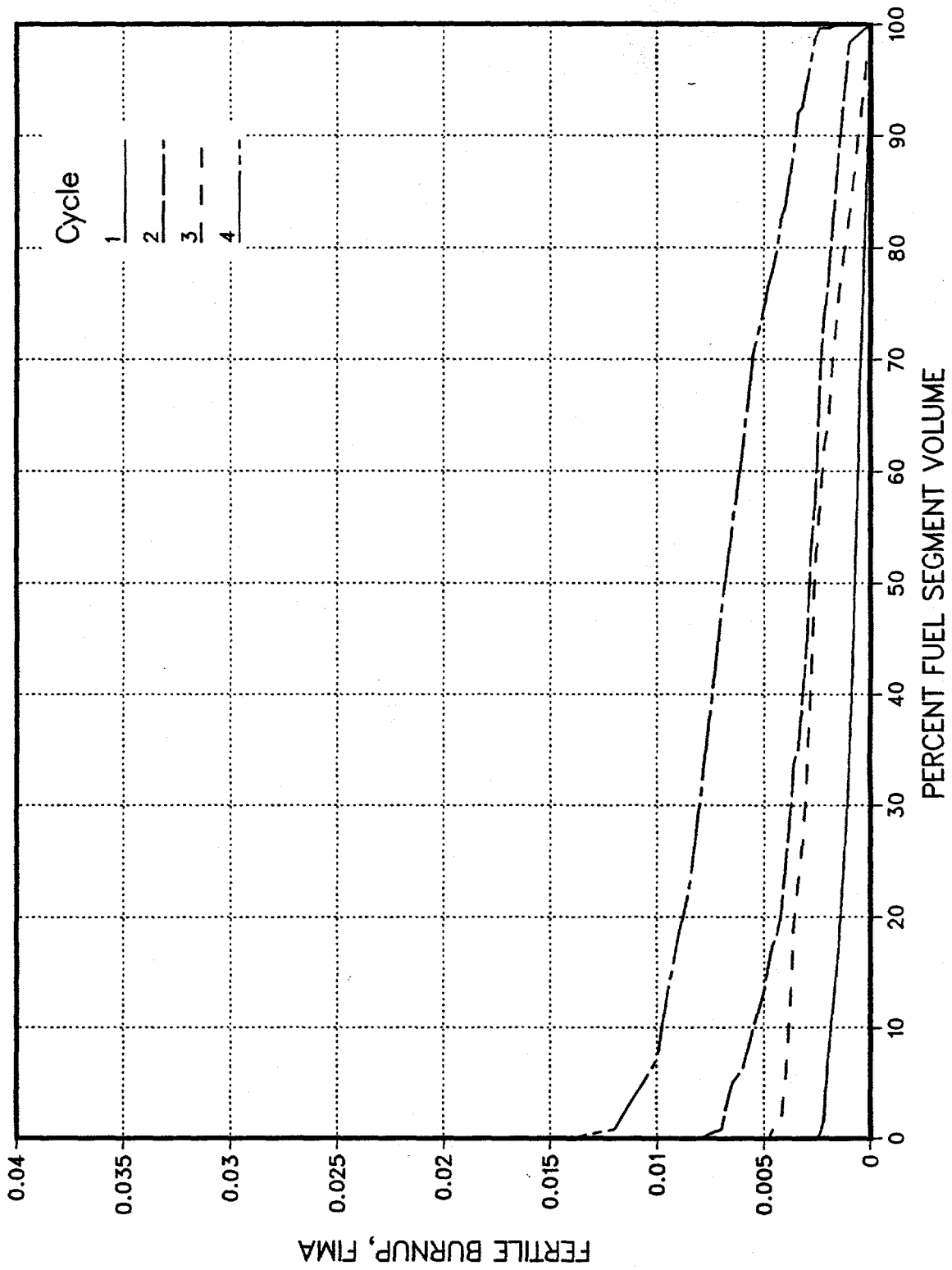

Figure 10
FISSILE BURNUP VOLUME DISTRIBUTIONS FOR SEGMENTS 3 AND 9

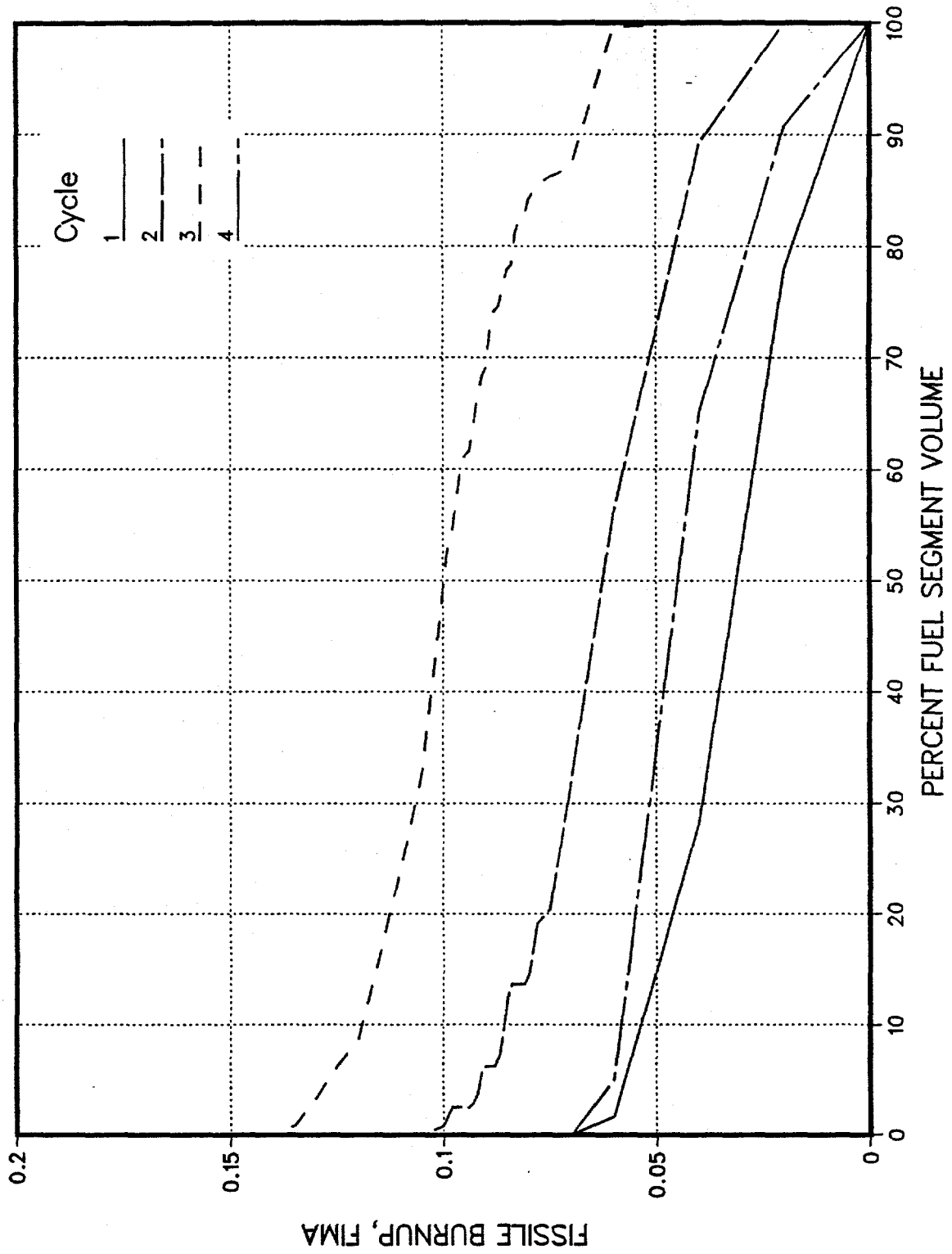

Figure 11

FERTILE BURNUP VOLUME DISTRIBUTIONS FOR SEGMNETS 3 AND 8

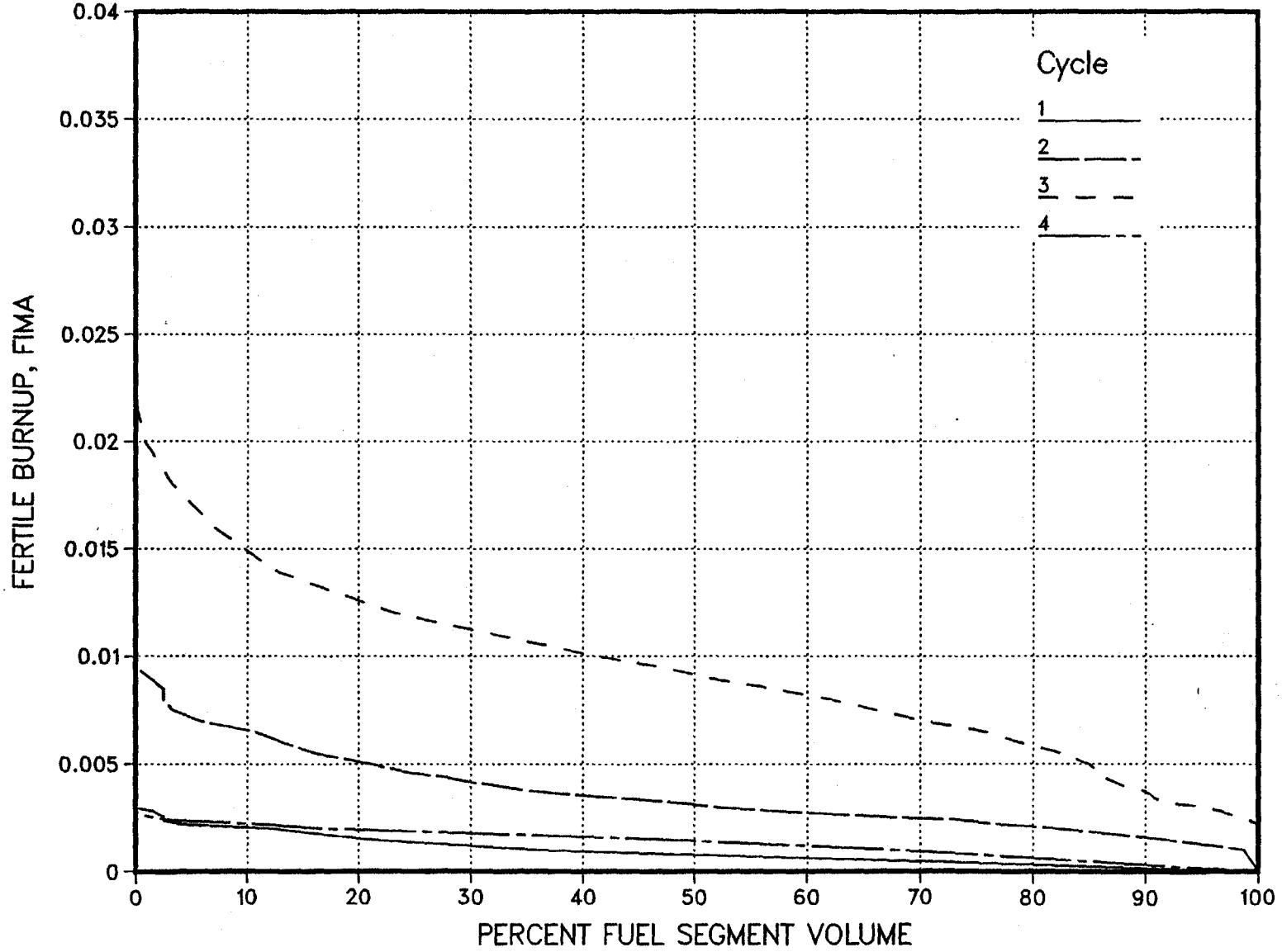

Figure 12
FISSILE BURNUP VOLUME DISTRIBUTION FOR SEGMENT 4

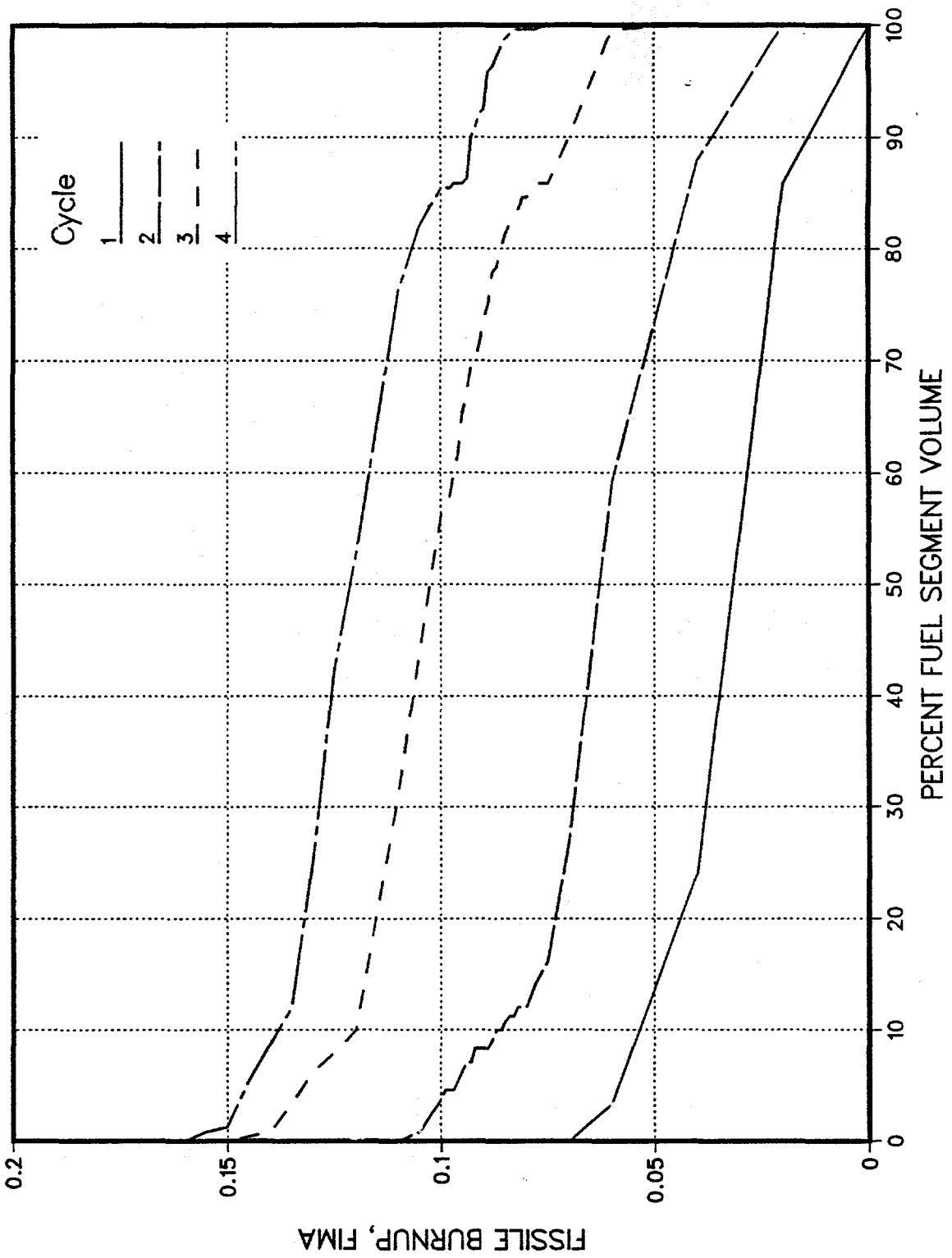

Figure 13
FERTILE BURNUP VOLUME DISTRIBUTION FOR SEGMENT 4

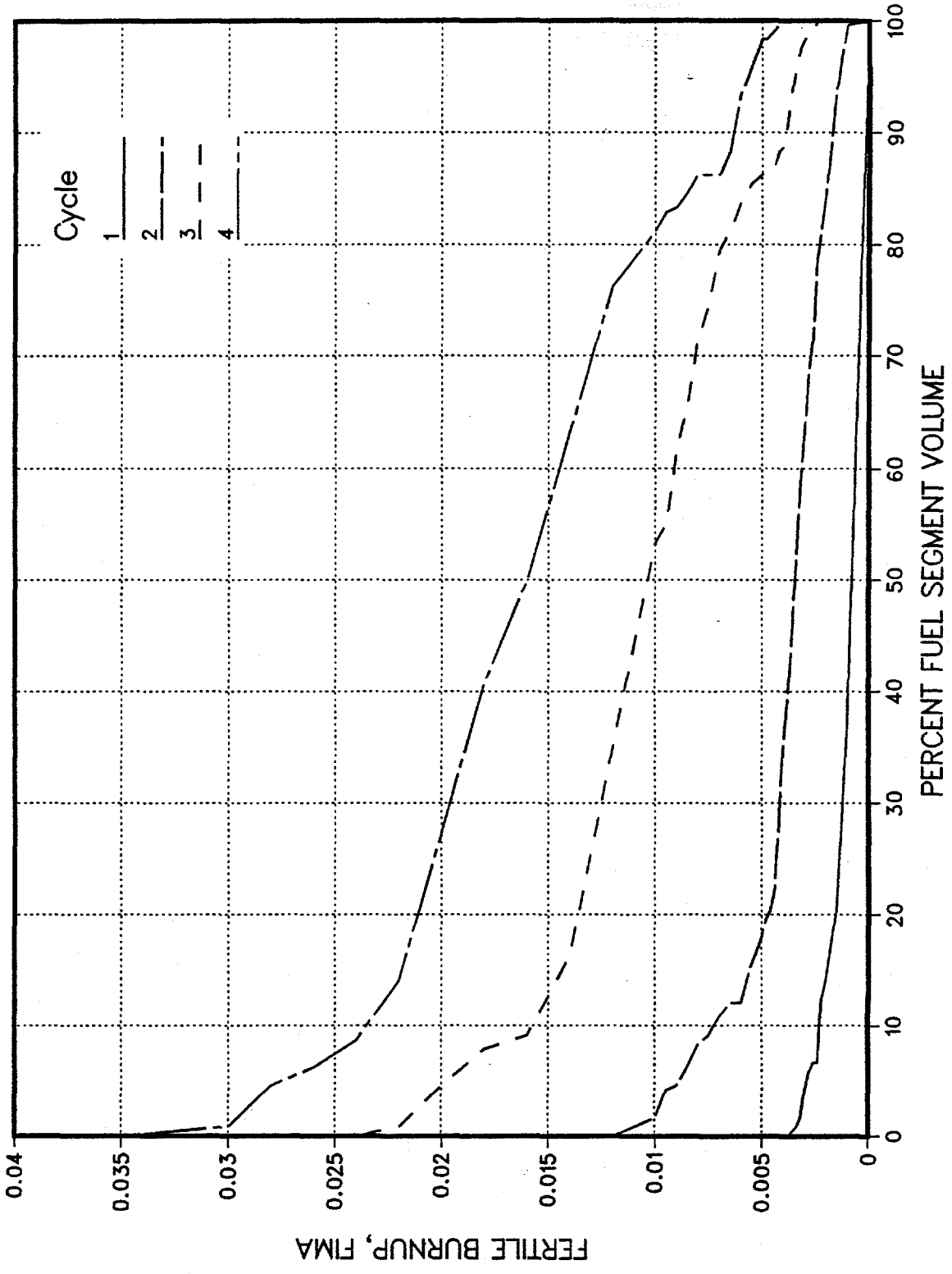

Figure 14
FISSILE BURNUP VOLUME DISTRIBUTION FOR SEGMENT 5

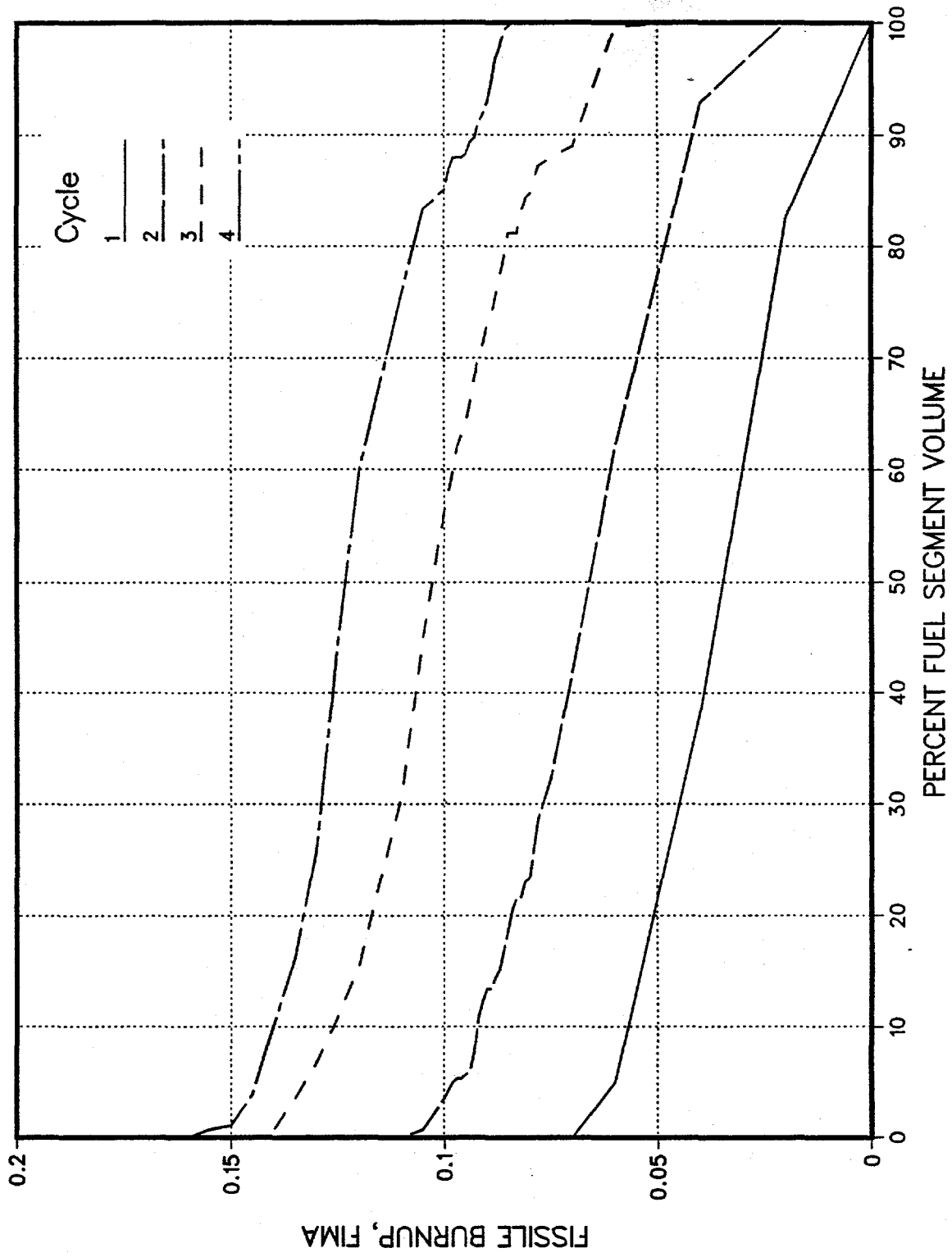

Figure 15
FERTILE BURNUP VOLUME DISTRIBUTION FOR SEGMENT 5

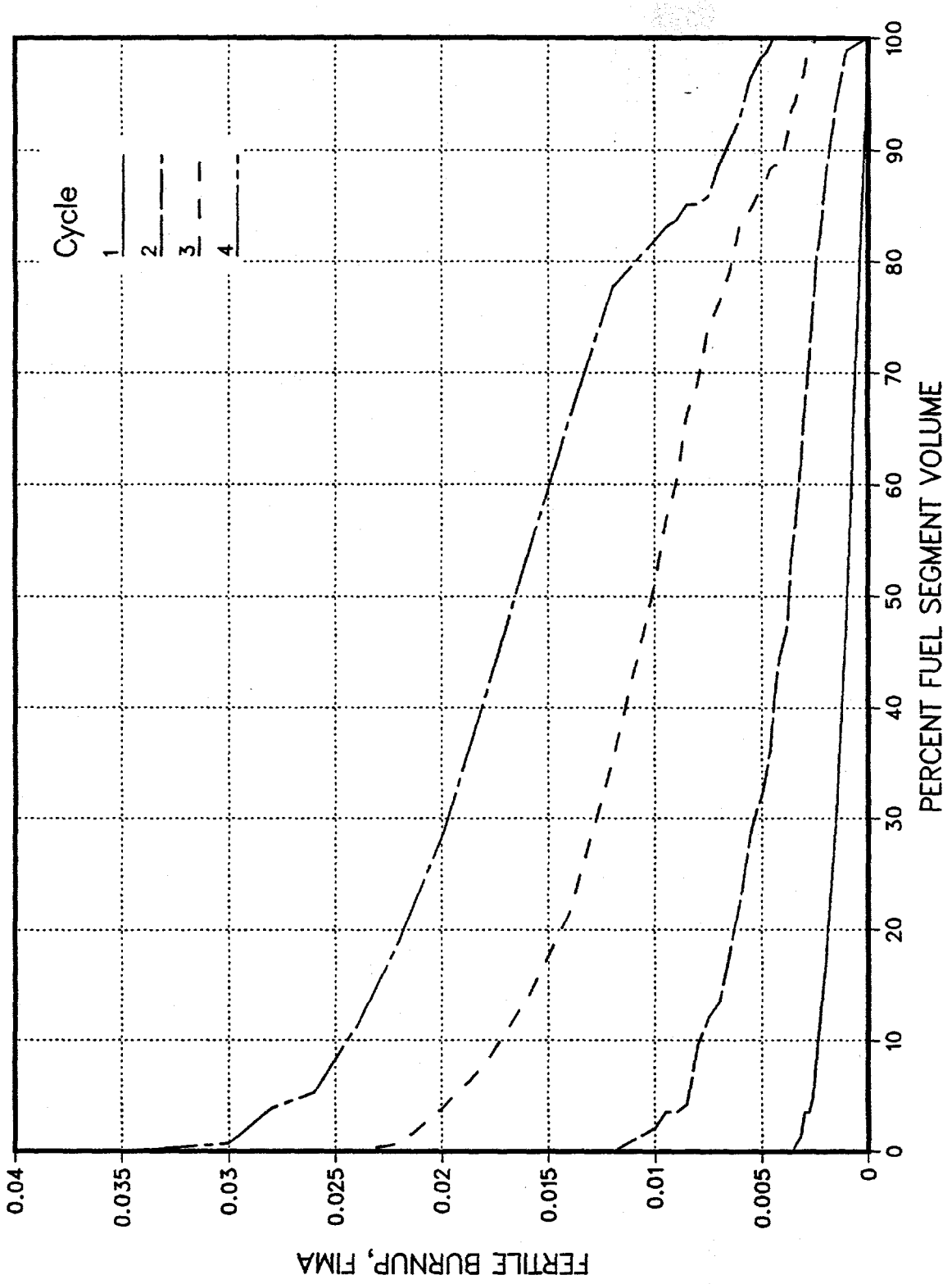

Figure 16
FISSILE BURNUP VOLUME DISTRIBUTION FOR SEGMENT 6

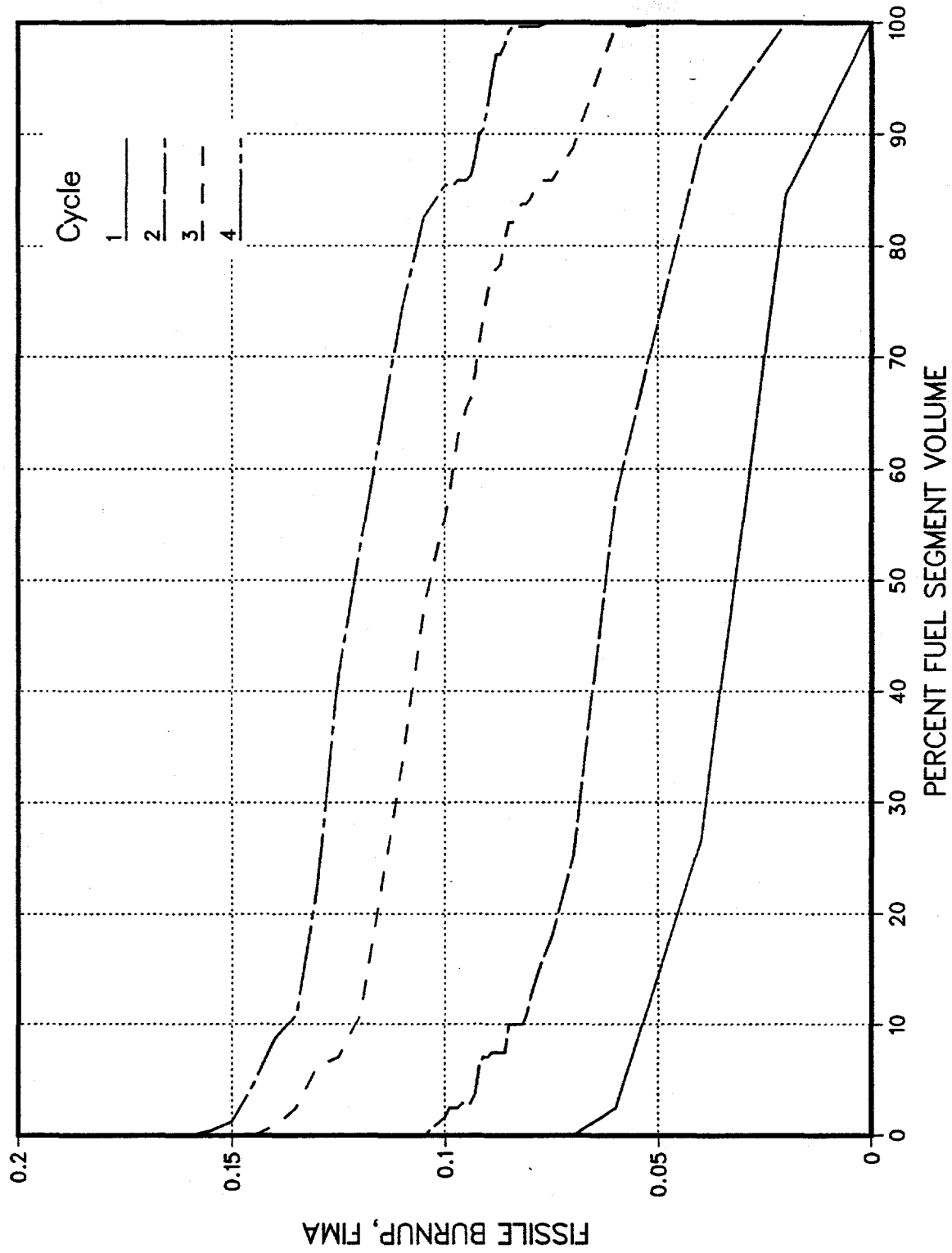

Figure 17
FERTILE BURNUP VOLUME DISTRIBUTION FOR SEGMENT 6

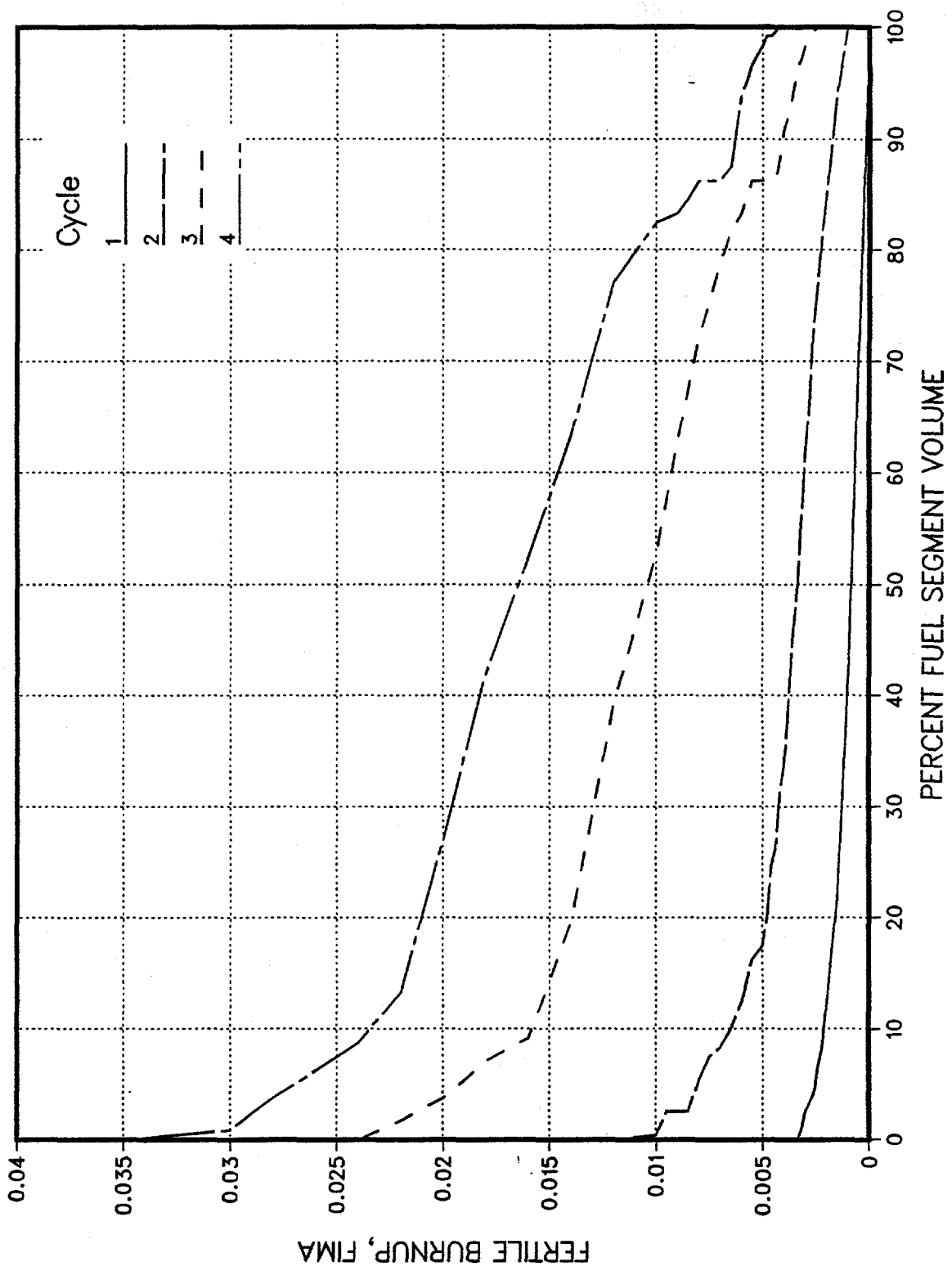

Figure 18
FAST NEUTRON FLUENCE DISTRIBUTIONS FOR SEGMENTS 1 AND 7

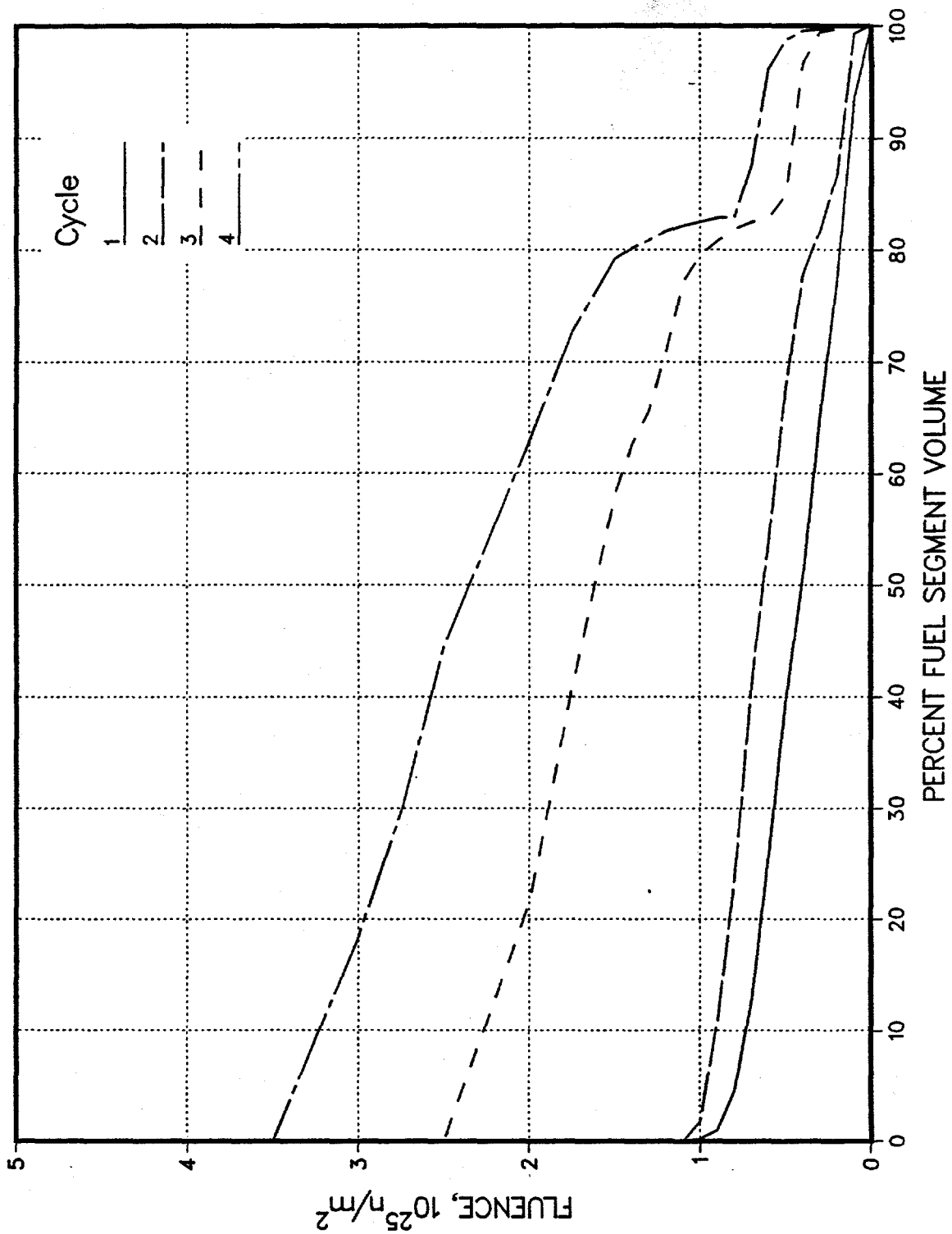

Figure 19
FAST NEUTRON FLUENCE DISTRIBUTIONS FOR SEGMENTS 2 AND 8

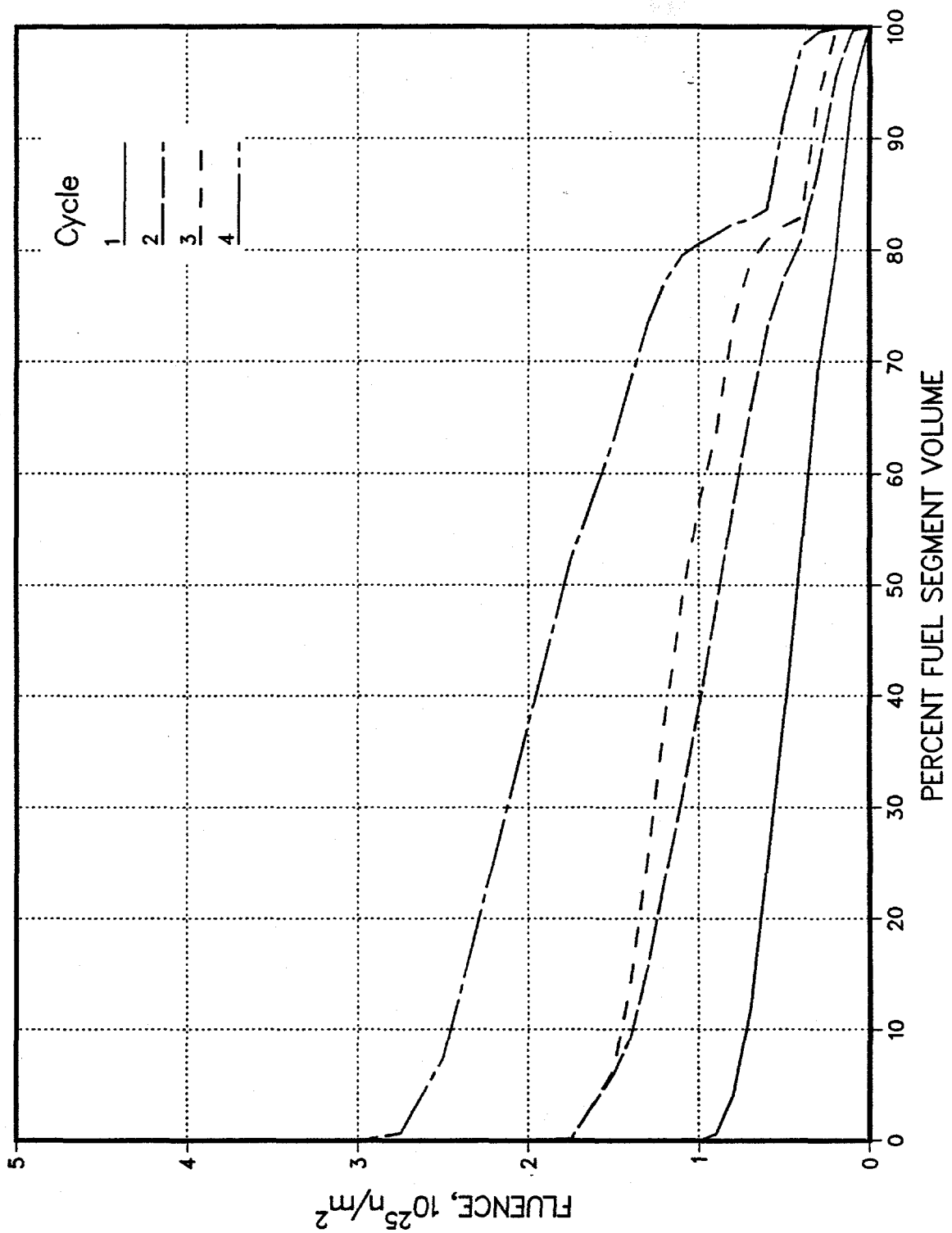

Figure 20
FAST NEUTRON FLUENCE DISTRIBUTIONS FOR SEGMENTS 3 AND 9

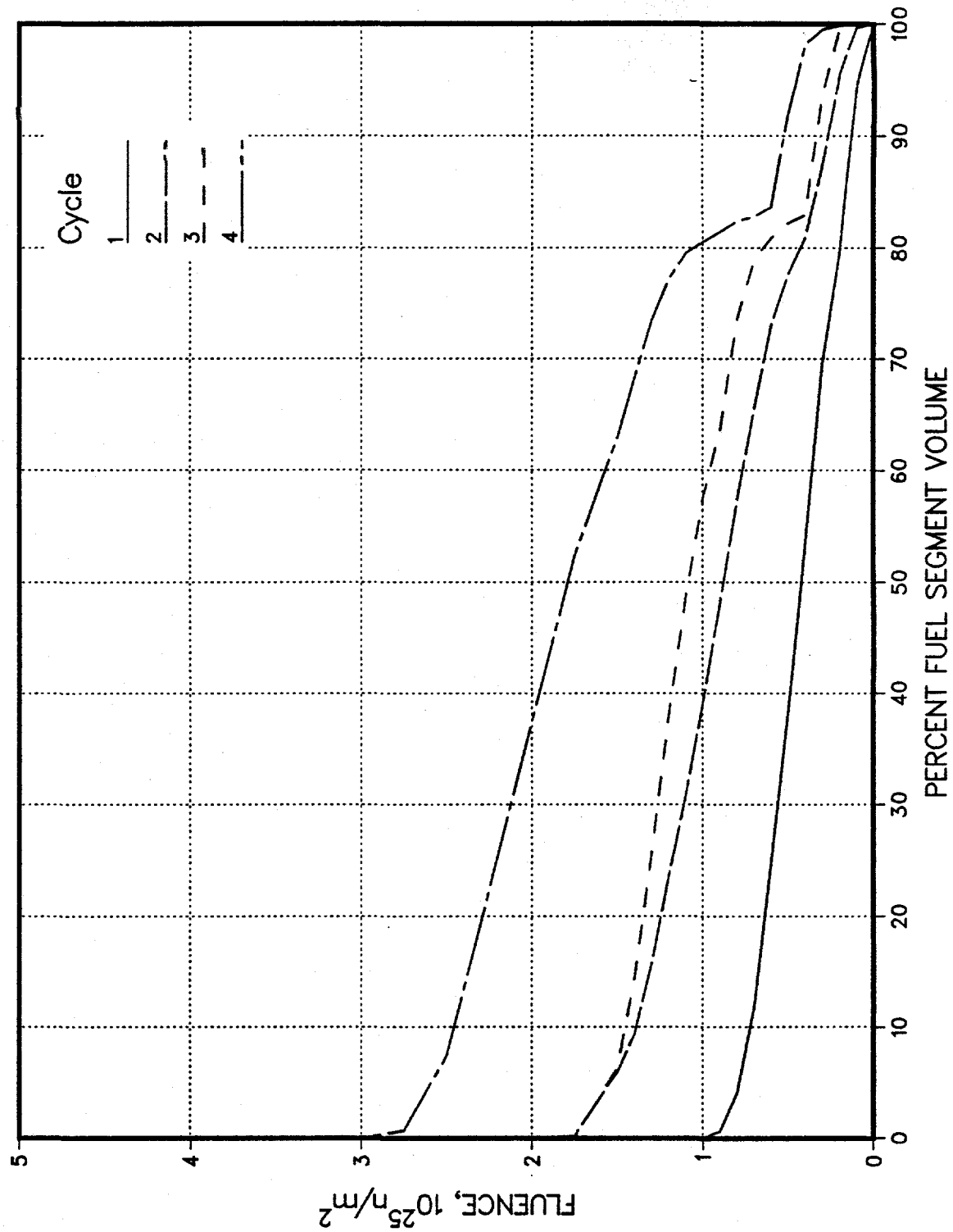

Figure 21
FAST NEUTRON FLUENCE DISTRIBUTION FOR SEGMENT 4

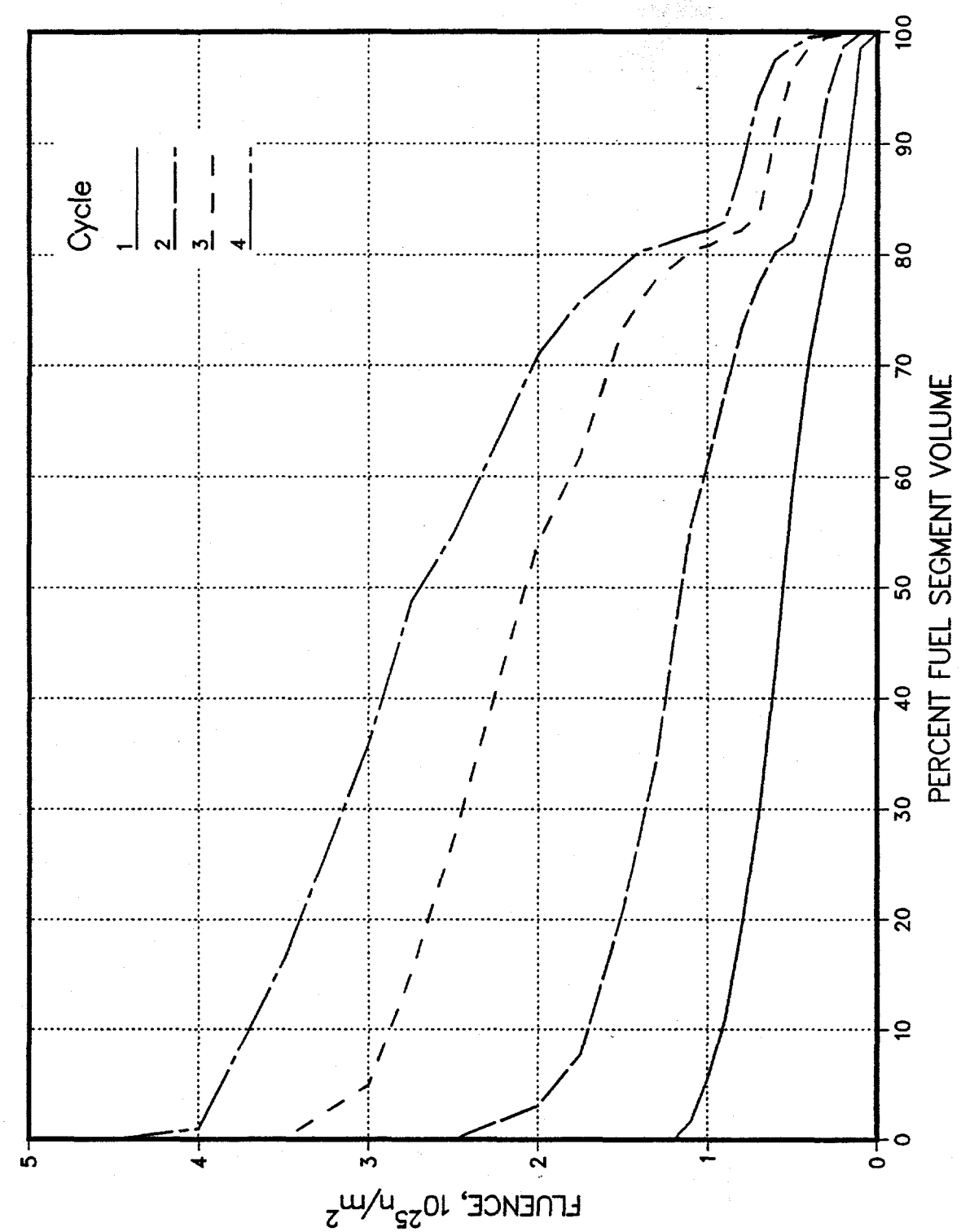

Figure 22
FAST NEUTRON FLUENCE DISTRIBUTION FOR SEGMENT 5

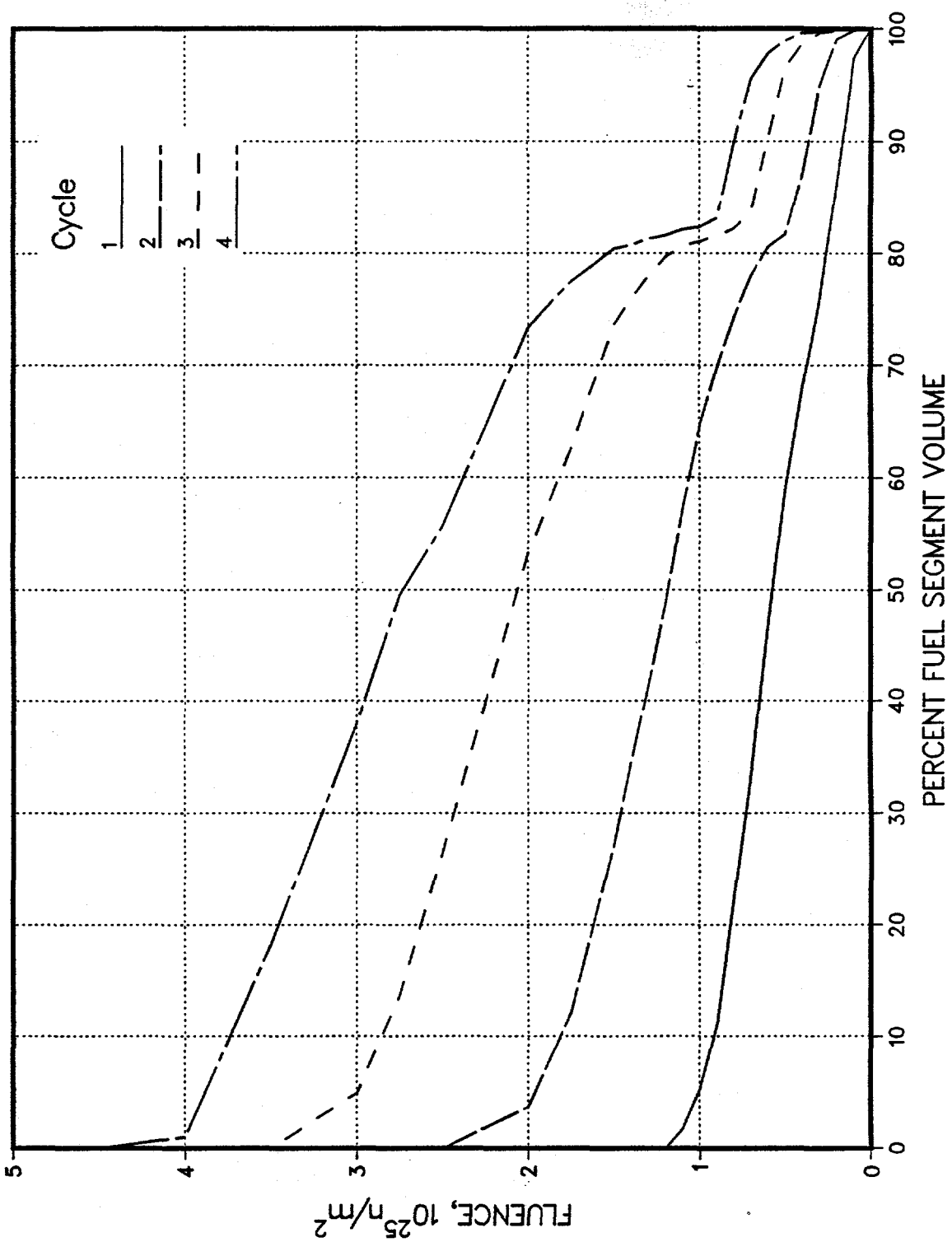

Figure 23
FAST NEUTRON FLUENCE DISTRIBUTION FOR SEGMENT 6

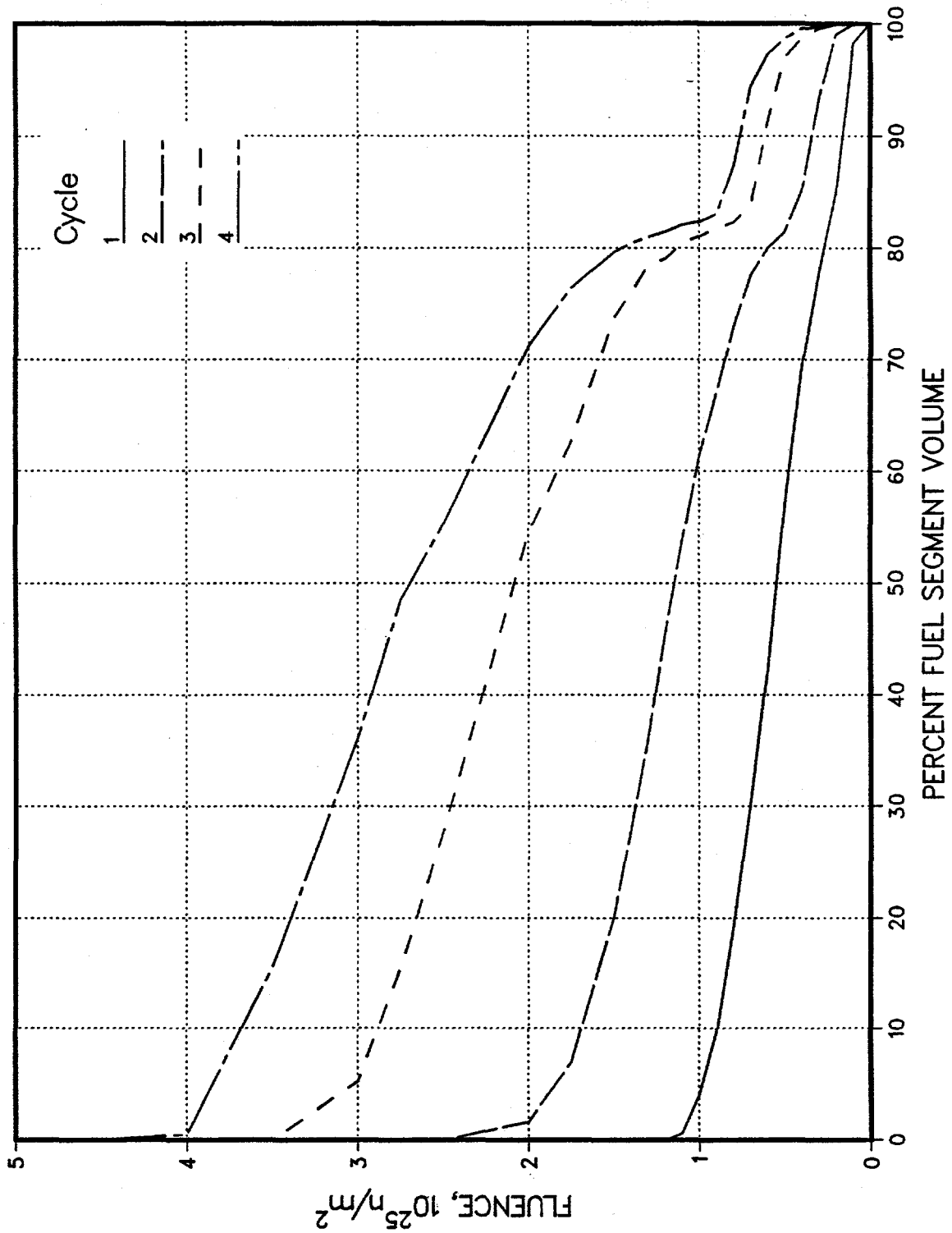

Figure 24
CORE-AVERAGED FISSILE FUEL FAILURE HISTORY

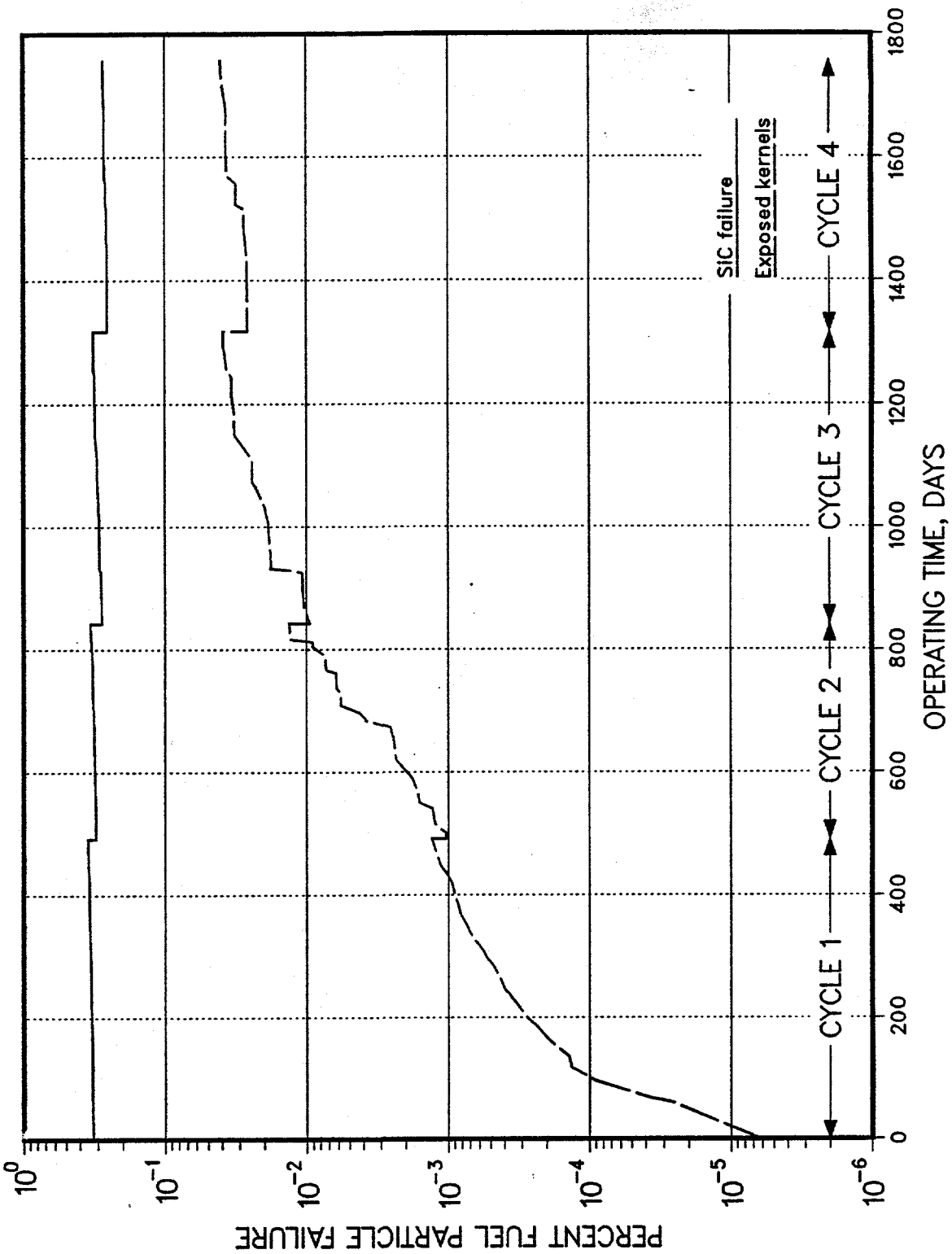

Figure 25
CORE-AVERAGED FERTILE FUEL FAILURE HISTORY

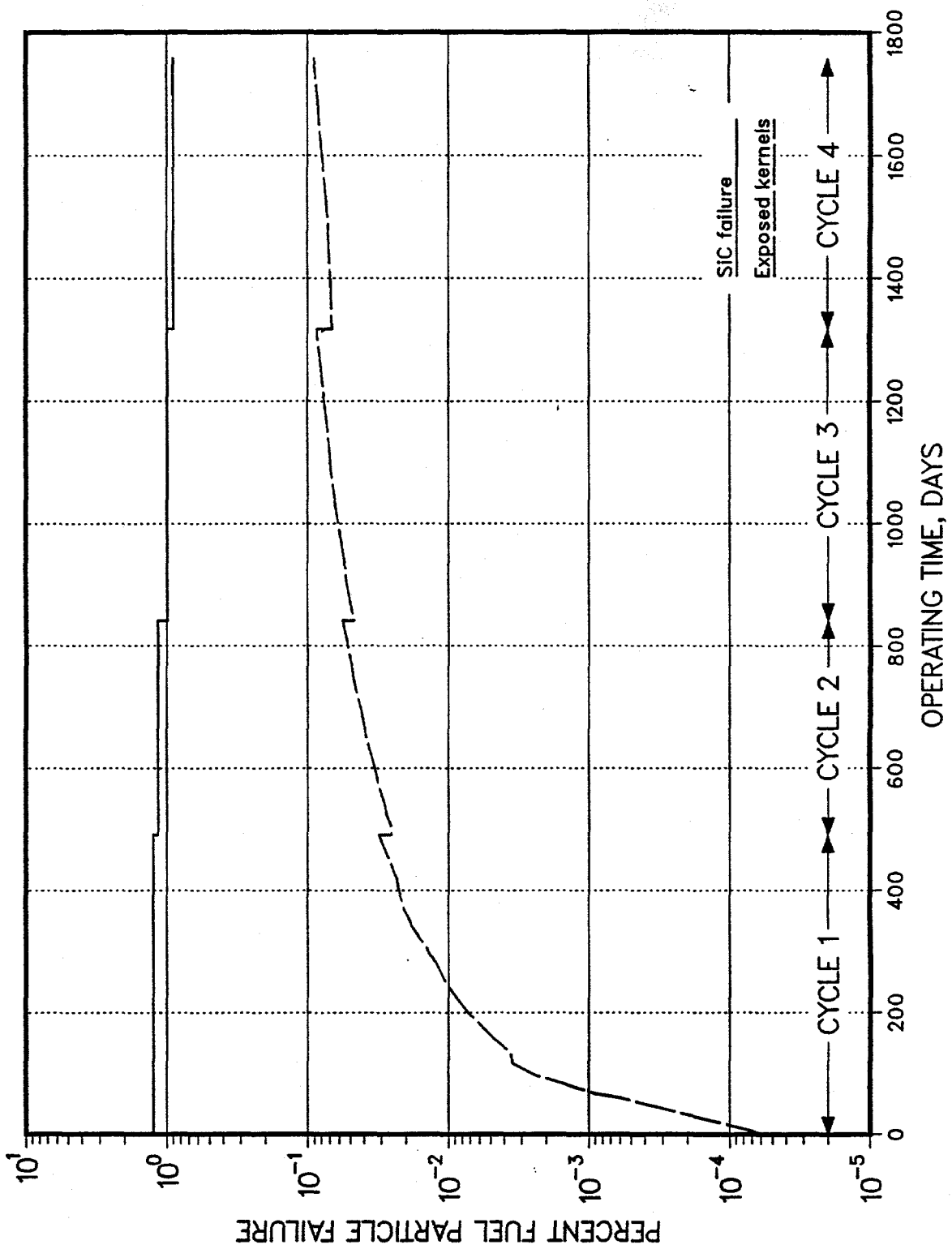

Figure 26
FSV PREDICTED CORE-AVERAGED Kr-85m RELEASE

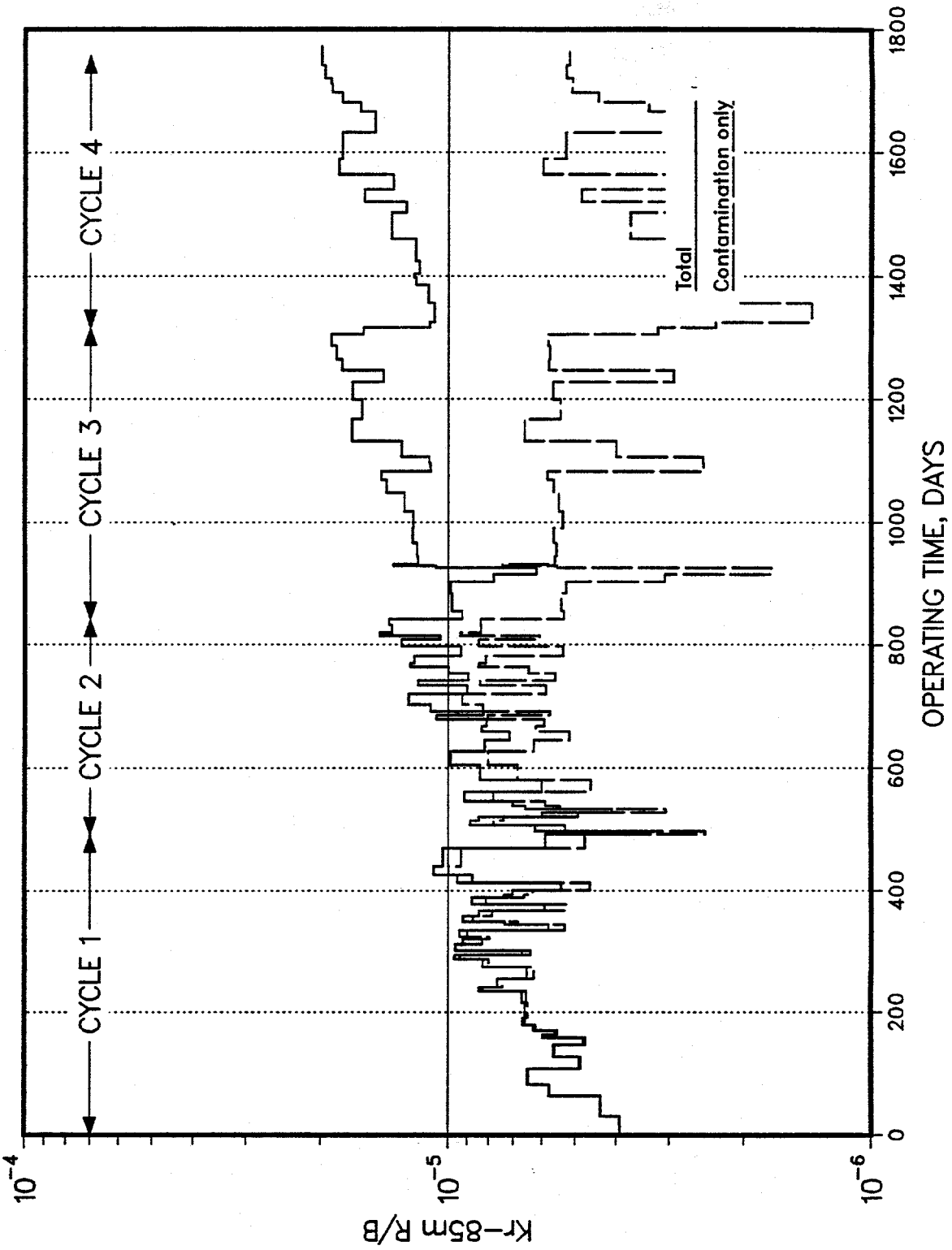

Figure 27
FSV PREDICTED CORE-AVERAGED Xe-138 RELEASE

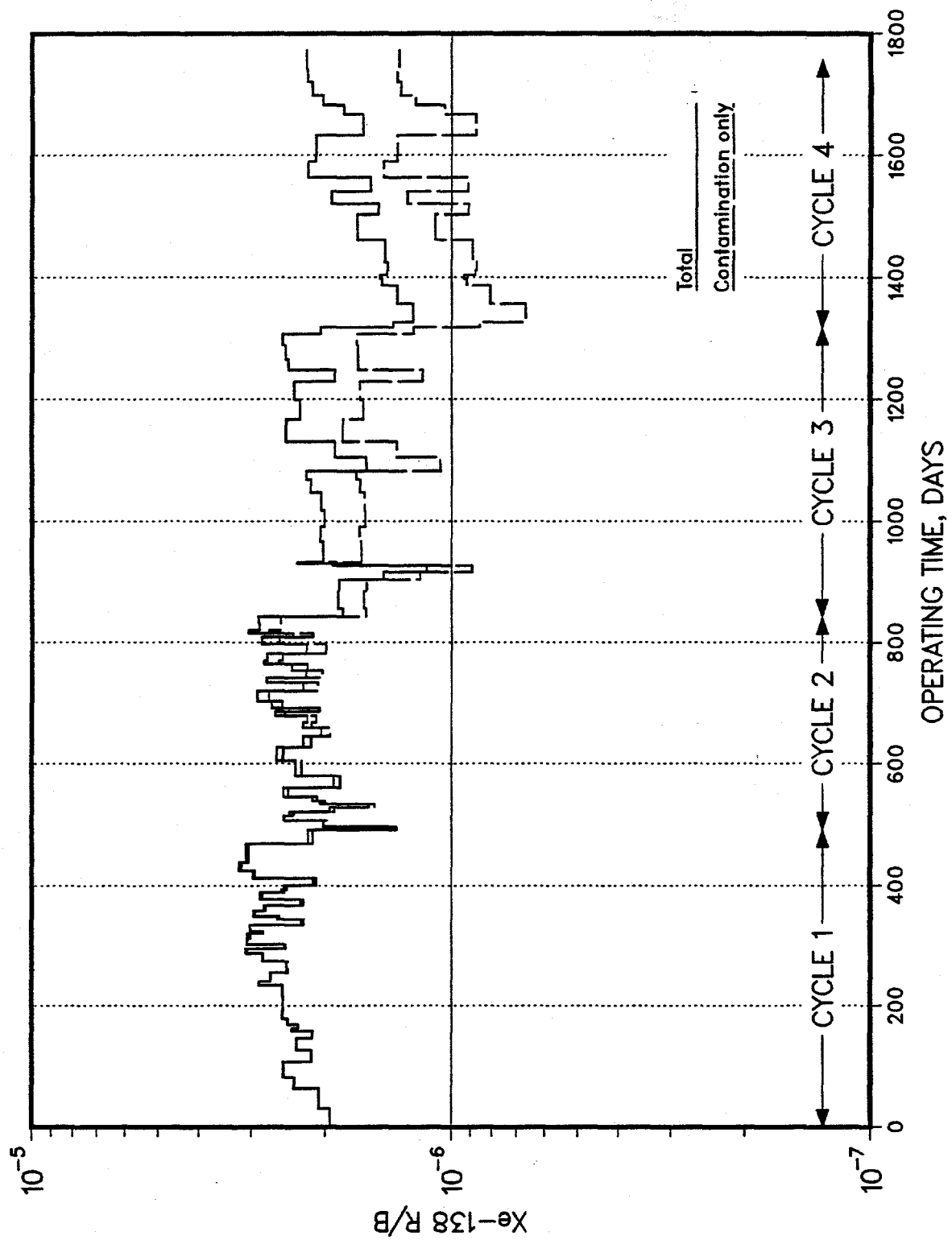

Figure 28

COMPARISON OF FSV PREDICTED AND MEASURED Kr-85m RELEASE

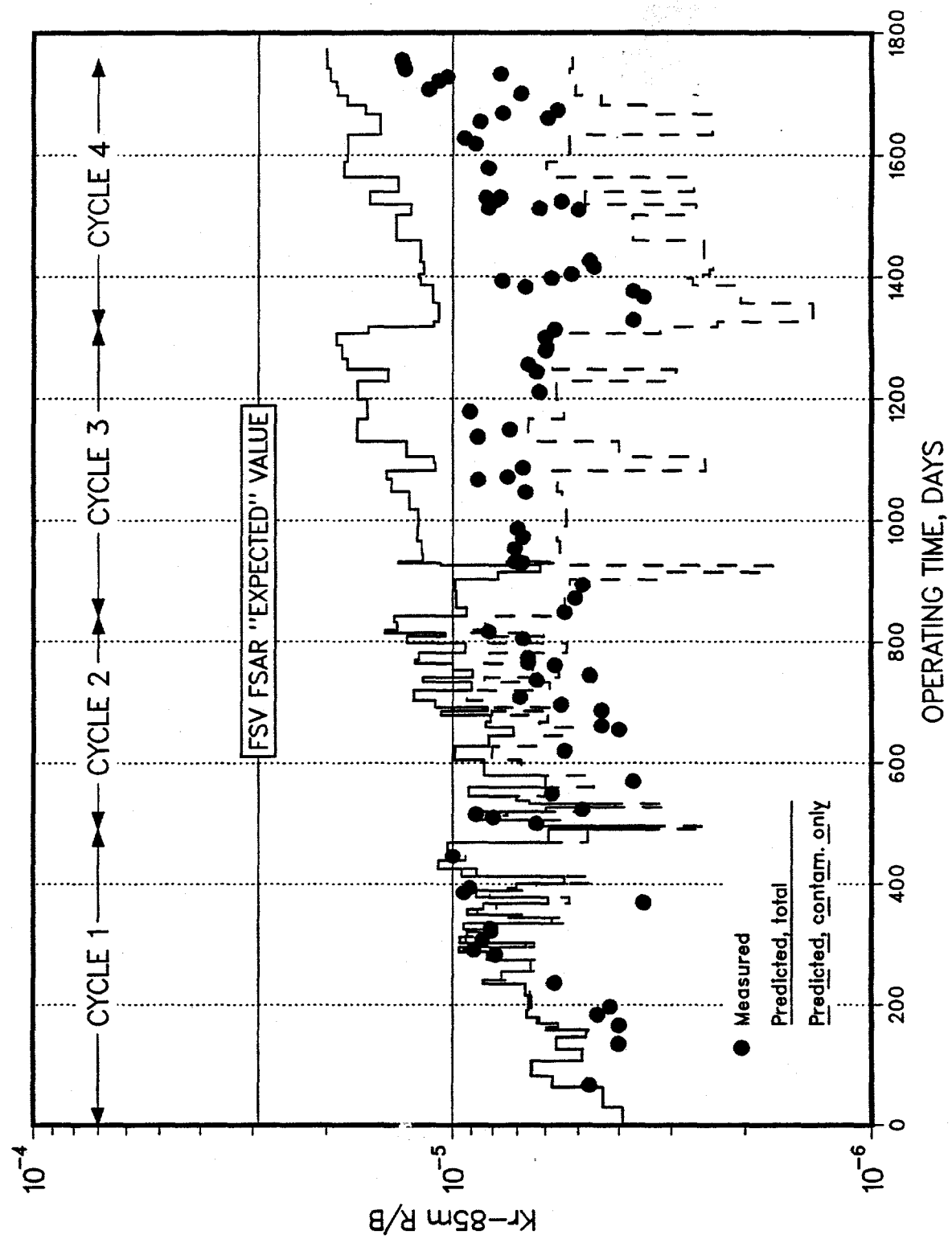

Figure 29

COMPARISON OF FSV PREDICTED AND MEASURED Xe-138 RELEASE